Batteries & Supercaps

Research Article
doi.org/10.1002/batt.202300595

Chemistry Europe
European Chemical Societies Publishing

www.batteries-supercaps.org

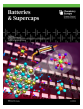

Elucidating Gas Evolution of Prussian White Cathodes for Sodium-ion Battery Application: The Effect of Electrolyte and Moisture

Sören L. Dreyer,[a] Faduma M. Maddar,[b] Aleksandr Kondrakov,[a, c] Jürgen Janek,[a, d] Ivana Hasa,*[b] and Torsten Brezesinski*[a]

As global energy storage demand increases, sodium-ion batteries are often considered as an alternative to lithium-ion batteries. Hexacyanoferrate cathodes, commonly referred to as Prussian blue analogues (PBAs), are of particular interest due their low-cost synthesis and promising electrochemical response. However, because they consist of ~50 wt% cyanide anions, a possible release of highly toxic cyanide gases poses a significant safety risk. Previously, we observed the evolution of $(CN)_2$ during cycling via differential electrochemical mass spectrometry (DEMS), but were unable to determine a root cause or mechanism. In this work, we present a systematical investigation of the gas evolution of Prussian white (PW) with different water content via DEMS. While H_2 is the main gas detected, especially in hydrated PW and during overcharge (4.6 V vs. Na^+/Na), the evolution of CO_2 and $(CN)_2$ depends on the electrolyte conductive salt. The use of oxidative $NaClO_4$ instead of $NaPF_6$ is the leading cause for the formation of $(CN)_2$. Mass spectrometric evidence of trace amounts of HCN is also found, but to a much lower extent than $(CN)_2$, which is the dominant safety risk when using $NaClO_4$-containing electrolyte, which despite being a good model salt, is not a viable option for commercial applications.

1. Introduction

Electrochemical energy-storage systems, such as rechargeable batteries, are at the heart of the energy transition, contributing to decarbonization of transport and grid energy storage.[1,2] Lithium-ion batteries (LIBs) have been intensively developed and commercialized to fulfil both application requirements, however the rising prices of the raw materials used for their production and supply constraints triggered an accelerated development of alternative battery chemistries.[3,4] Sodium-ion batteries (SIBs), which can be manufactured using the same process equipment as LIBs, are therefore developed as a complementary technology, especially for use cases where cost factors play a more important role than energy density.[5–8] Several cathode active material (CAM) families have been proposed for SIBs, including layered oxides, polyanionic compounds, and Prussian blue analogues (PBAs).[9–11] The latter ones are considered particularly promising due to their low-cost synthesis methods, eliminating the need for high temperature treatments, their tunable redox behavior achieved through the use of sustainable and abundant metals, such as iron and manganese, and their satisfactory capacity and power capability conferred by their open framework structure with large interstitial sites enabling 3D diffusion pathways while minimizing volume changes upon cycling.[9,12,13] Furthermore, they can be operated both in aqueous electrolytes, with a limited cell voltage, and in organic electrolytes similar to those for LIBs, thereby realizing higher cell voltages.[14–18] Strong research and commercialization efforts for these materials are therefore underway, including manufacturers, such as CATL, Natron Energy, and Altris.[19,20]

PBAs for SIBs present the general formula of $Na_xM_a[M_b(CN)_6]_{1-y}\square_y{\cdot}zH_2O$, where M_a and M_b are transition metals, x ($0<x<2$), sometimes instead written as $2-x$, denotes the sodium content of the as-synthesized material, y ($0<y<1$) represent the content of $M_b(CN)_6$ vacancies symbolized as $\square$, and z the number of lattice water molecules per PBA unit.[14,15,18] The Na- and Fe-rich structures are often referred to as Prussian white (PW), indicating all iron to be fully reduced (Fe^{2+}/Fe^{2+}). Vacancies, sodium content, and water play a crucial role in the chemistry of these materials. Three main types of water molecules are present in the structure of PBAs, including chemically bonded coordinated water, interstitial water, and adsorbed water, which all affect their Na^+ storage behavior and cause side reactions with the electrolyte, leading to capacity

[a] S. L. Dreyer, Dr. A. Kondrakov, Prof. J. Janek, Dr. T. Brezesinski
Battery and Electrochemistry Laboratory (BELLA), Institute of Nanotechnology, Karlsruhe Institute of Technology (KIT), Hermann-von-Helmholtz-Platz 1, 76344 Eggenstein-Leopoldshafen, Germany
E-mail: torsten.brezesinski@kit.edu

[b] Dr. F. M. Maddar, Dr. I. Hasa
WMG, The University of Warwick, Coventry CV4 7AL, United Kingdom
E-mail: ivana.hasa@warwick.ac.uk

[c] Dr. A. Kondrakov
BASF SE, Carl-Bosch-Str. 38, 67056 Ludwigshafen, Germany

[d] Prof. J. Janek
Institute of Physical Chemistry & Center for Materials Research (ZfM/LaMa), Justus-Liebig-University Giessen, Heinrich-Buff-Ring 17, 35392 Giessen, Germany

Supporting information for this article is available on the WWW under https://doi.org/10.1002/batt.202300595

fading.[10,21–24] Therefore, for best CAM performance, a high Na content, but low fraction of vacancies and water, is desirable.[6] In recent years, many studies have been reported on optimized composition,[25–27] synthesis procedures,[28–34] drying procedures,[23,24,26,33,35] and chelating agents[36–40] to obtain PBA/PW materials with such properties. At the same time, various characterization methods and *in-situ* experiments have been employed to study the composition and behavior of PBA/PW materials during electrochemical cycling, mostly focusing on the evolution of crystal phases in dependence of state of charge (SOC) and water content.[41,42] Some of us have shown that an optimal dehydration process for the composite electrodes obtained by a more sustainable aqueous processing is even more critical when compared to the sole CAM powders.[43]

Various electrolyte solvent and salt combinations in PBA/PW-based cells have been reported and reviewed in the literature, with $NaPF_6$[21–23,26,35,40,43–47] and $NaClO_4$[24,25,27,29–34,36–39,48–56] being the most widely used conductive salts. Common solvents are organic carbonates, such as ethylene carbonate (EC), propylene carbonate (PC), dimethyl carbonate (DMC), diethyl carbonate (DEC), and combinations thereof, often also including the additive fluoroethylene carbonate (FEC).[57–59] For a PBA CAM, Piernas-Muñoz *et al.* reported a comparison of various solvent and salt combinations and electrode binders, finding 1 M $NaPF_6$ in EC:PC:FEC 49:49:2 to show the best performance in terms of specific capacity and capacity retention, and in this electrolyte, polyvinylidene difluoride (PVDF), closely followed by carboxymethyl cellulose (CMC), to be the best-performing binder.[60] However, the performance of $NaClO_4$-electrolytes was only slightly different, and the choice of electrolyte, salt, and additives also affects the anode material, electrolyte handling, and considerations related to safety and cost.[61–63]

Glycol ethers, such as diglyme, are another family of possible solvents, which generally lead to the formation of a more stable solid electrolyte interphase (SEI) both in half- and in full-cell configuration when compared to carbonates. In addition, when combined with PW cathodes, their lower anodic stability is not limiting, as PW operates within the electrochemical stability window of glymes.[64] In general, the formation and composition of both SEI and cathode electrolyte interphase (CEI) strongly depend on the chosen salt and solvent combinations.[57,58,65,66]

During battery operation, reactions of and between electrode materials and electrolyte, such as the SEI formation or the release of lattice oxygen from charged layered oxides, with subsequent oxidation of electrolyte, result in gas evolution, which can be studied *in-situ* via differential electrochemical mass spectrometry (DEMS).[67–70] While the gas evolution of LIBs has been studied in great detail, investigations of SIB gassing are still relatively sparse.[67,69,71,72] In previous works on high-entropy PBA and PW CAMs for SIBs, some of us have performed DEMS measurements, in which not only the commonly evolved gases H_2 and CO_2, but also cyanogen [$(CN)_2$] (assumed to be the product of oxidative dimerization of CAM anions, similar to the release of O_2 from layered oxides) were observed.[48–50,67] This finding, although at a lower level, was recently confirmed by Geisler.[72] At the same time, Li *et al.* observed the release of both hydrogen cyanide (HCN) and $(CN)_2$ during thermal runaway of PBA-based cells, and $(CN)_2$ release during the thermal decomposition of PBA/PW has previously been reported.[46,73]

While $(CN)_2$ finds some application as a fumigant and in organic synthesis, it forms HCN upon hydrolysis and also *in vivo*, resulting in an acute toxicity only slightly lower than that of HCN itself.[74–76] The observation of these gases challenges the perception of PBA/PW as being non-toxic and raises safety concerns regarding SIBs using such CAMs. This is especially relevant when considering overcharge events, both intentional and unintentional, and application in confined and poorly ventilated spaces, as commonly found in stationary energy-storage systems located in basements, server rooms, etc.[10,41,46,77]

In this work, we elucidate the role of carbonate solvents, conductive salts, and water content on the gas evolution of aqueous processed PW cathodes, investigated via DEMS during cycling and overcharge. By using a $Na_{1.80(5)}Fe[Fe(CN)_6]\cdot 1.84(3)H_2O$ PW CAM with Fe as the only transition metal and studying it in optimized electrodes of high areal loading,[43] any observation can be understood as genuinely deriving from the material properties and not as immediate artifacts, e.g. from the presence of other metals in the previously studied high-entropy materials[48–50] or from the use of small-scale material and electrode preparation and handling (more prone to the introduction of impurities). Overall, it is found that H_2 is the main gas detected, with CO_2 and $(CN)_2$ evolution strongly depending on the electrolyte conductive salt and its oxidative nature. The use of $NaClO_4$ is the leading cause for the formation of $(CN)_2$, especially during overcharge, which however is not a commercially viable electrolyte salt.

2. Results and Discussion

2.1. Initial Gassing Measurements and Considerations

In this study, DEMS measurements were performed on PW/Na-metal cells cycled at 0.1 C rate (14 mA g^{-1}) in the potential window of 2.0–4.0 V vs. Na^+/Na for two cycles, reflecting regular cycling conditions, and then between 2.0 and 4.6 V in a third cycle, reflecting an overcharge scenario (see more details in Experimental section). It should be noted that due to the two-electrode cell setup, the reported potentials may be affected by SEI formation on the Na-metal anode.[72] Detailed conditions for each measurement presented can be found in Table S1 (Supporting Information), with a summary of the respective specific charge/discharge capacities obtained and gas amounts detected given in Table S2 (Supporting Information).

The initial set of experiments consisted on the comparison of the gassing behavior of PW/Na-metal cells employing two commonly used electrolyte solutions in SIB research, i.e. 1 M $NaClO_4$ in EC:PC:DMC = 1:1:1 (v/v/v) with 5 v% FEC and 1 M $NaPF_6$ in EC:DEC = 3:7 (v/v). While the first one, used in previous DEMS studies on PBAs/PW,[48–50] constitutes a more

Research Article
doi.org/10.1002/batt.202300595
Chemistry Europe
European Chemical Societies Publishing

academic approach involving the use of $NaClO_4$ salt, the second one resembles a more industrially relevant electrolyte employing $NaPF_6$. However, these two electrolytes serve as model electrolytes to investigate different gas evolution mechanisms induced by chemically different salts and solvents when cycling dehydrated PW electrodes. Figure 1a and b displays the gas evolution obtained over two initial cycles and an overcharge event during the third cycle. While almost the same capacities and voltage profiles are obtained (see values in Table S2 and Figure S1a, Supporting Information), the gassing behavior differs significantly.

During regular cycling, H_2 evolution is observed for the cell containing $NaClO_4$-electrolyte only at the onset of the first charge process, while it is observed during the whole first charge with a maximum peak at the end of the de-sodiation at 4.0 V, and to a lower extent also at the end of the second charge for the cell containing $NaPF_6$-electrolyte.

In both cases, the formation of H_2 is most likely associated to reduction of residual electrolyte moisture at the anode side. In addition, coordinated water in the PW, which cannot be removed during dehydration, leads to potential further water release in the form of $Na(OH_2)^+$ into the electrolyte during de-sodiation, and particularly so at the end of charge, where the coordination becomes weaker.[33,78] Loosely bound lattice water is likely released fully in the initial cycle, explaining the early H_2 evolution onset, specifically in the first cycle. The larger amount of H_2 detected for the cell containing $NaPF_6$-electrolyte can be explained considering the additional hydrolysis of $NaPF_6$, yielding acidic conditions due to HF formation, which is then further reduced to H_2 at the anode.[79–82] In the cell containing $NaClO_4$-electrolyte, on the other hand, no acid formation is occurring, and the reduction of water at the sodium metal leaves OH^- anions behind. These, in turn, lead to basic electrolyte conditions and hydrolysis of EC and other organic carbonates, which results in CO_2 evolution and explains the stronger evolution of CO_2 in the cell containing $NaClO_4$-electrolyte during regular cycling within the stability window of the solvent molecules.[83,84] The decomposition of surface carbonate impurities,[67,85,86] which have recently been shown to be present also on PW materials,[21] may also contribute to CO_2 evolution and explain the weak signal observed for the cell containing $NaPF_6$-electrolyte. In the absence of lattice oxygen, no chemical oxidation of electrolyte by reactive species released from the lattice may occur. However, the electrochemical oxidation of EC has been shown to occur at potentials above ~4.6 V vs. Li^+/Li, i.e. ~4.3 V vs. Na^+/Na, providing an explanation for the strong

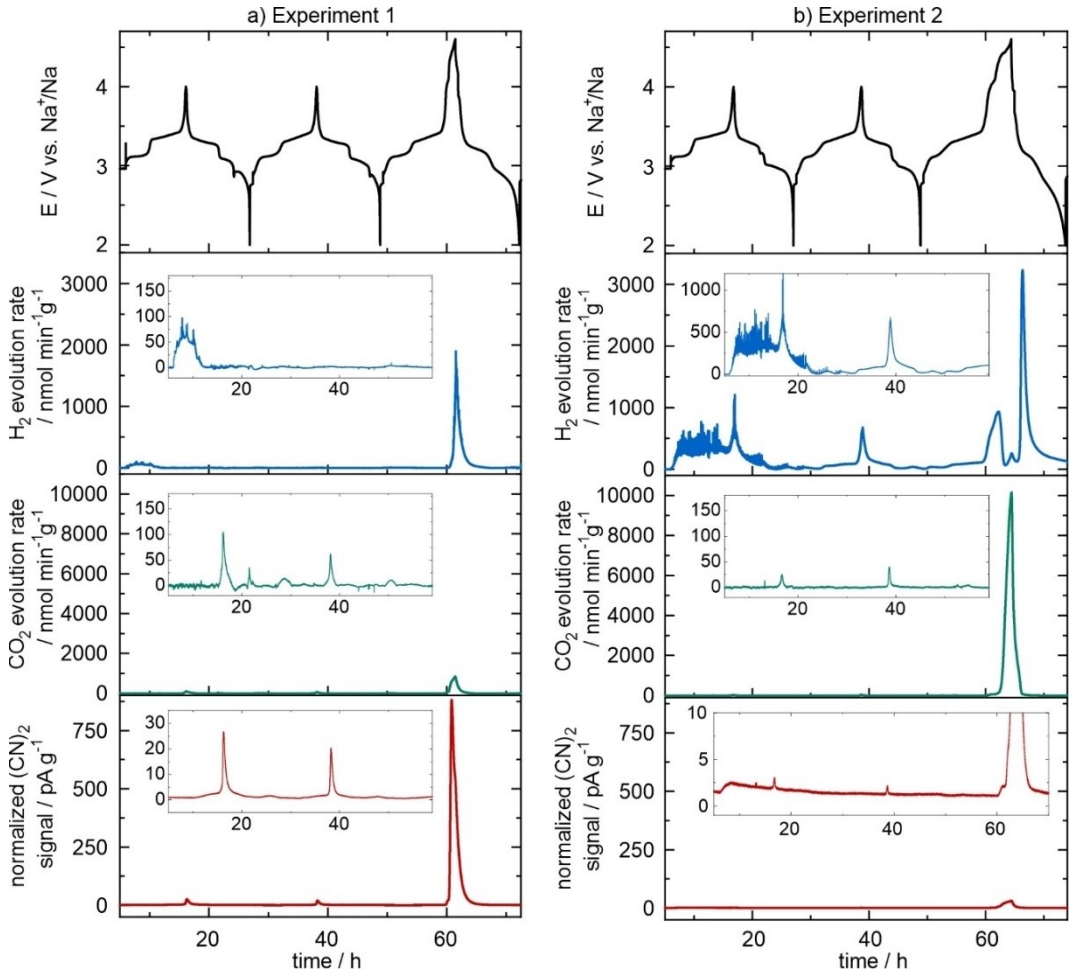

Figure 1. Gas evolution detected in Na half-cells using a dehydrated PW cathode in two different electrolytes: (a) 1 M $NaClO_4$ in EC:PC:DMC = 1:1:1 (v/v/v) with 5 v% FEC and (b) 1 M $NaPF_6$ in EC:DEC = 3:7 (v/v).

CO_2 evolution during overcharge.[79,87] The drastic difference in CO_2 evolution rates during overcharge is due to the presence of the more oxidation-sensitive DEC[88] in the $NaPF_6$-electrolyte, as will be shown in section 2.3. It should also be noted that the overall time at high potentials is higher for the cell containing $NaPF_6$-electrolyte (3.6 h charge above 4.0 V vs. 1.4 h for the cell containing $NaClO_4$-electrolyte), as can be seen from the direct comparison of voltage profiles in Figure S1a (Supporting Information). Concurrent H_2 evolution during overcharge is caused not only by remaining coordinated water, but also by the electrochemical oxidation of electrolyte, as protic oxidation products are reduced at the anode.[89] The observed suppression of H_2 evolution for the DEC-containing electrolyte during peak CO_2 evolution is likely due to displacement of the former by the latter in carrier gas. The effect is particularly noticeable in the ionization within the mass spectrometer, where a decrease even in carrier gas signal is detected due to high CO_2 concentration. As will be shown in section 2.3., this displacement only occurs in the presence of strongly CO_2-evolving DEC.

Lastly, the evolution of cyanogen, i.e. $(CN)_2$, is also reported for both measurements. Shown is $m/z = 52$, but the fragments and heavier isotope species at $m/z = 26$, 27, and 53 are detected too (see section 2.6.). Since unfortunately no calibration gas is available for this compound in He, a conversion of the measured signal to an absolute gas amount is not directly possible. For a single measurement, detector currents may be reported,[48,90,91] but a semi-quantitative normalization by both CAM mass and spectrometer calibration sensitivity has to be applied to allow comparisons between different measurements.[92] In the mass spectrometer, each species' ion current is amplified using a secondary electron multiplier (SEM) instead of a Faraday cup detector. With a signal gain of around 3 decades, this allows for trace detection and distinction from background noise in the first place. However, especially in newly installed SEMs, such as the one used for this study, aging and degradation lead to a decrease in ion current and SEM gain over time, which can be roughly adjusted for by spectrometer bake-out and applying a higher voltage.[93–95] Since both H_2 and CO_2 signals are also amplified by the SEM, their calibration sensitivity, i.e. the slope of their calibration curves, is known, and a relative comparison can be made between the slopes of each gas for various measurements. The $(CN)_2$ signal is then normalized between measurements by this relative factor, as detailed in Figure S2a and b, Table S3 (Supporting Information), and the literature.[50] In this study, factors between 0.71 and 1.37 have been applied to yield the reported normalized $(CN)_2$ signals. As shown in Figure 1a and b and Figure S1b (Supporting Information), in all cycles, a difference far greater is observed between the $(CN)_2$ evolution in the two electrolytes, with a factor of 26 and 28 between peak currents during regular cycling and overcharge, respectively. In both cases, $(CN)_2$ evolution is observed at high SOC and potential near the end of charge, yet the evolution is far stronger for the cell containing $NaClO_4$-electrolyte, and during regular cycling hardly visible against the background for the cell containing $NaPF_6$-electrolyte.

To confirm the observed gas evolution trends, repeat measurements were conducted, as shown in Figure S3 (Supporting Information). $NaClO_4$-containing electrolyte (Figure S3a, Supporting Information) was prepared freshly in an attempt to both ensure repeatability over electrolyte batches and reduce the H_2 evolution at the onset of cycling. As a result, the H_2 evolution is suppressed and the CO_2 evolution during regular cycling is reduced, further confirming the effect of residual moisture in the electrolyte as the main source for water. Again, $(CN)_2$ evolution was observed, especially during overcharge for the $NaClO_4$-electrolyte. A deviation of the peak normalized $(CN)_2$ signal by a factor of ~2 (881 pA g^{-1} vs. 414 pA g^{-1}) demonstrates that, while there are limitations of the presented semi-quantitative normalization, the uncertainties obtained are an order of magnitude smaller than the difference between the two electrolytes. We note that this repeat measurement was carried out five months after the first measurement and, to adjust for the aforementioned SEM degradation, with 1380 V instead of 1200 V applied to the SEM. Figure S3b (Supporting Information) shows that for a repeat measurement (in this case, shortly after the initial measurement) on a cell containing the $NaPF_6$-electrolyte, similar gas evolution profiles were obtained, with the only variations observed in the total amount of gas generated during overcharge, which depends strongly on the exact duration of the overcharge and electrode specific surface area.

As oxidation of cyanide anions is required to form $(CN)_2$, the presence of the ClO_4^- anion with its oxidative properties appears to be an explanation for the formation of cyanogen. Metzger *et al.* previously reported CO_2 evolution stemming from the oxidation of conductive carbon by $LiClO_4$ at potentials higher than 5 V vs. Li^+/Li.[87] However, $(CN)_2$ signal is also observed during overcharge for the cell containing $NaPF_6$-electrolyte, and because different cell sets were used, $NaClO_4$ contamination can be ruled out. Therefore, either a competing or a more complex mechanism must occur, such as one involving a previous release of CN^- and/or HCN or involving iron. Possible considerations include the roles of SOC and potential as oxidation causes, as well as the roles of water content, electrolyte solvents, acidity/basicity, and various experimental settings in the gas evolution. These will be disentangled in the following in order to understand the gassing behavior of PW CAM better and narrow down the root cause of $(CN)_2$ evolution during overcharge above 4.0 V.

The analysis will focus on H_2, CO_2, and $(CN)_2$. Two other species commonly discussed in gas evolution studies are CO ($m/z = 28$) and C_2H_4 ($m/z = 26$ and 28), with the former formed together with CO_2 during electrolyte decomposition and the latter generated during SEI formation from EC.[67–70] Indeed, as shown in Figure S4a (Supporting Information), a strong $m/z = 28$ signal is observed during overcharge. However, CO is also formed as a fragment of CO_2 or DEC in the mass spectrometer, which has to be corrected for. Additionally, a correction for C_2H_4 is needed, which is also present in the calibration gas and can normally be analyzed at $m/z = 26$ as $C_2H_2^+$, yet not in the case of PW, as $m/z = 26$ is dominated by the CN^+ fragment or $(CN)_2^{2+}$ ions. A precise quantitative determination of CO would

Research Article
doi.org/10.1002/batt.202300595
Chemistry Europe
European Chemical Societies Publishing

only be possible via differential electrochemical infrared spectroscopy (DEIRS).[90] Since the evolution of CO typically occurs concurrently with that of CO_2 and from the same underlying electrolyte oxidation mechanisms, it is therefore not reported individually. This is also shown in Figure S4a (Supporting Information), where after correction for the CO fragment of CO_2 no remaining signal (but also no negative signal) is observed during regular cycling, because hydrolysis of EC and decomposition of Na_2CO_3 do not generate CO.[83,84] Nevertheless, during overcharge a signal of genuine CO from electrolyte oxidation remains after correction.

POF_3 ($m/z = 85$ and 104) is detected as the product of $NaPF_6$ hydrolysis and decomposition, also yielding highly reactive PF_5, which however was found to further decompose to POF_3 in the steel tubing leading to the mass analyzer.[80–82] As shown in Figure S4b (Supporting Information), POF_3 can indeed be detected from the cell containing $NaPF_6$-electrolyte. However, its traces are too dilute in the constant carrier gas stream of the open headspace DEMS setup used in this work, and therefore no precise measurement outside of overcharge conditions is possible.[67]

2.2. Effect of Water Content

By using undried electrodes as described previously,[43] the effect of interstitial and adsorbed water on gas evolution is studied, as shown in Figure 2a for a cell containing $NaClO_4$-electrolyte and in Figure 2b for a cell containing $NaPF_6$-electrolyte. In both cases, gas evolution peaks appear broader, with a distinctive different voltage profile associated to the electrochemical activity of the monoclinic PW phase exhibiting lower capacities within the standard 2.0–4.0 V potential range. As expected, a strong H_2 evolution is now observed even during regular cycling for the cell containing $NaClO_4$-electrolyte. The release of water into the electrolyte upon charge results in increased EC hydrolysis, thus also increasing the CO_2 evolution. The $(CN)_2$ evolution, on the other hand, is reduced when compared to that of the dehydrated electrode, so that a dependence of $(CN)_2$ evolution on SOC and sodium content in the structure can be assumed. The same findings apply also during overcharge. It is worth mentioning that the hydrated monoclinic PW phase enables extraction of one sodium per formula unit at about 3 V *vs.* Na^+/Na and that the water content of the structure shifts the potential for the low-spin iron to almost 4 V vs. Na^+/Na. Rudola *et al.* reported that accessing this

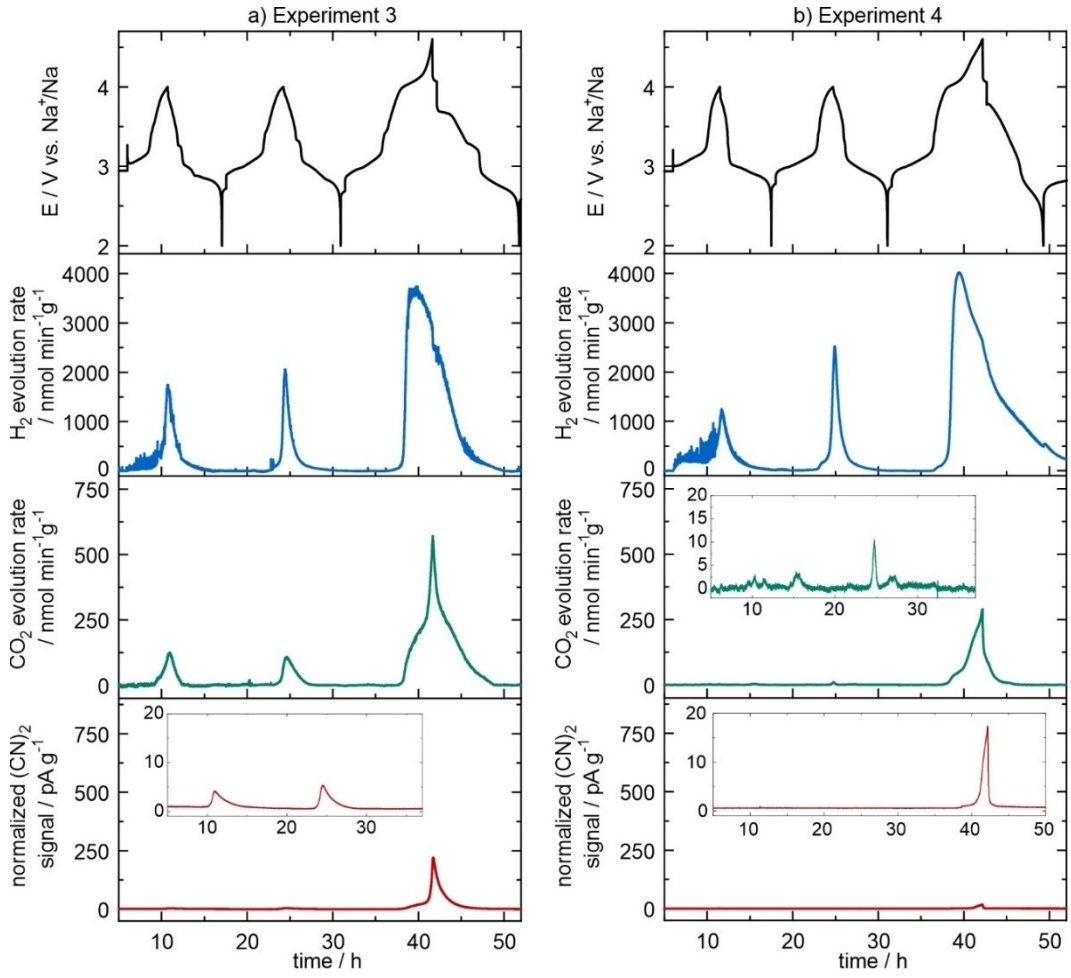

Figure 2. Gas evolution in Na half-cells with an undried PW cathode using two different electrolytes: (a) 1 M $NaClO_4$ in EC:PC:DMC = 1:1:1 (v/v/v) with 5 v% FEC and (b) 1 M $NaPF_6$ in EC:DEC = 3:7 (v/v).

plateau rapidly degrades the cell performance, as further structural water is released.[96] However, for the cell containing $NaPF_6$-electrolyte, the first-cycle H_2 evolution appears similar as with the dehydrated electrode, with a rather constant H_2 evolution starting immediately upon passing current through the cell and only becoming more intensive near the end of charge. In the second cycle, the H_2 evolution is then similar between both electrolytes, demonstrating the dominating role of PW water content. Because the electrolyte is acidic due to PF_6^- hydrolysis, no CO_2 evolution from EC hydrolysis is observed, as this would require basic conditions. Under regular cycling conditions, only a weak $(CN)_2$ signal is detected. Interestingly, a different overcharge behavior is evident for this electrolyte with an undried electrode, with now H_2 evolution from water release (similar to the other electrolyte) dominating the gas evolution instead of CO_2 from DEC oxidation. Likely, the presence of water or more acidic conditions affects the DEC oxidation and explains the lower CO_2 evolution. The $(CN)_2$ evolution is again suppressed, both compared to the combinations of either $NaPF_6$-electrolyte and dehydrated electrode or $NaClO_4$-electrolyte and undried electrode. Regarding mechanistic considerations, the reduced evolution at the same potential when compared with dehydrated electrodes rules out an electrochemical oxidation as the rate limiting step, while the reduced evolution at lower SOC might indicate a contribution of chemical oxidation.

At this point, two effects of increased water content shall be discussed. At high potentials and water contents (undried electrodes), and especially during overcharge, one might assume water oxidation to occur via electrocatalysis by the desodiated PW framework,[97] yet no O_2 evolution was detected, as shown in Figure S5a and b (Supporting Information). The high H_2 evolution amounts, i.e. curve integrals as listed in Table S2 (Supporting Information), can be converted into water loss from the CAM, as exemplified in Table S4 and Figure S6 (Supporting Information), yielding a water release between 1.15 and 1.37 wt % during regular cycling and 4.93 to 6.44 wt% during overcharge. This is in good agreement with the ~10 wt% total water content of undried PW or water uptake of dry material often observed via thermogravimetric analysis, highlighting the importance of PW dehydration to mitigate the risk of cell swelling and rupture due to H_2 accumulation.[21,22,24,43,51] As is shown in Table S5 (Supporting Information), an average weight loss of 10.43 wt% relative to the CAM mass was observed when drying the electrodes used in this study (i.e. difference in water content between undried and dried electrodes).

2.3. Effect of Electrolyte Solvent

The effect of electrolyte solvents on gas evolution was also investigated. To this end, 1 M $NaPF_6$ in EC:PC:DMC = 1:1:1 (v/v/v) with 5 v% FEC was prepared and data were obtained for both dehydrated and undried PW electrodes. These data can then be evaluated in comparison with the results obtained by using 1 M $NaPF_6$ in EC:DEC = 3:7 (v/v) (Figure 1b and 2b), but this time avoiding the strong CO_2 evolution of DEC. The solubility of $NaClO_4$ in EC:DEC = 3:7 (v/v) was found to be unsatisfactory at room temperature, while at higher temperatures degradation was observed in the form of turbidity and dark precipitate, thus the $NaClO_4$ version of this electrolyte was not investigated.

As shown in Figure 3a, the combination of a dehydrated PW electrode and the new electrolyte resulted in no significant H_2 evolution during regular cycling, indicating a lower water content when compared with Figure 1b. Possible reasons include a lower moisture level in the freshly prepared electrolyte than that shipped before use or a reduced release of interstitial and adsorbed water into the electrolyte containing different solvents. By contrast, slightly stronger CO_2 evolution and $(CN)_2$ evolution were observed. During overcharge, it becomes apparent that the change of electrolyte solvents, i.e. the replacement of DEC, strongly affects the gassing behavior, as Figure 3a no longer shows the strong CO_2 evolution and displacement of H_2 evolution found in Figure 1b for EC:DEC. Instead, the evolution of these gases is now similar in profile and quantity to that of Figure 1a, where the same solvent mixture, but a different conductive salt, was used, suggesting that under overcharge conditions, the electrochemical oxidation of solvent molecules is the main contribution to the evolution of these gases. On the other hand, the $(CN)_2$ evolution remained low, similar to that in Figure 1b, highlighting that it is not the choice of solvent, but of conductive salt, that affects the $(CN)_2$ release.

Figure 3b shows the gassing resulting from a combination of an undried PW electrode and the newly prepared electrolyte. The H_2 evolution is drastically increased when compared with the dehydrated electrode in Figure 3a and similar to that observed for undried electrodes in Figure 2. The CO_2 evolution during regular cycling is increased when compared with that in Figure 2b and 3a (slightly), indicating that the solvent mixture may be more prone to hydrolysis of the organic carbonates. A very weak $(CN)_2$ release is observed during regular cycling, but interestingly the evolution is the strongest out of all $NaPF_6$-containing measurements reported in this study. A possible explanation other than cross-contamination for this observation is discussed in section 2.7.

We note that an analysis using diglyme as electrolyte solvent, as reported by Geisler,[72] was attempted but proven unsuccessful, since it was quickly purged out by the carrier gas stream, leaving a cell too dry to cycle behind. Because the same effect is observed with organic carbonate solvents when using polypropylene instead of glass fiber separators, a possible explanation is the weaker retention of an electrolyte reservoir, akin to poor wetting.

2.4. Effect of Conductive Salt

Having narrowed down the reason for strong $(CN)_2$ evolution from PW to the use of $NaClO_4$ as conductive salt, two hypotheses regarding its role may be made, i.e. either the oxidative nature of $NaClO_4$ results in an increased oxidation of CN^- to $(CN)_2$ or the electrolyte acidity/basicity (the former from

Research Article
doi.org/10.1002/batt.202300595
Chemistry Europe
European Chemical Societies Publishing

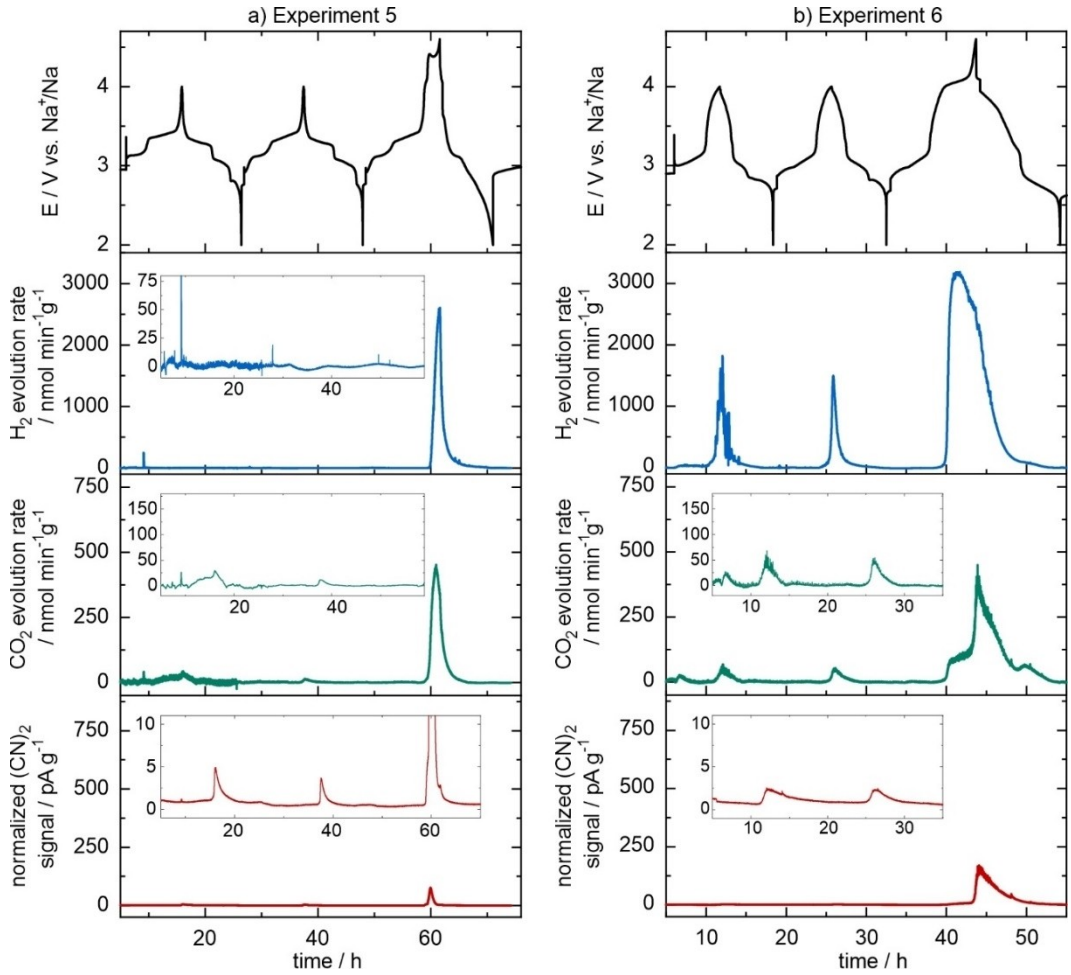

Figure 3. Gas evolution in Na half-cells with (a) a dehydrated and (b) undried PW cathode using 1 M $NaPF_6$ in EC:PC:DMC = 1:1:1 (v/v/v) with 5 v% FEC as electrolyte.

$NaPF_6$ and the latter from $NaClO_4$, as discussed previously) influences the $(CN)_2$ evolution, with basic conditions favoring it. To differentiate the two hypotheses, two additional electrolytes were prepared, both based on the previously used EC:PC:DMC mixture containing 5 v% FEC. The first electrolyte contained 0.3 M $NaClO_4$, the other 0.3 M $NaClO_4$ and 0.7 M $NaPF_6$, with the respective DEMS results shown in Figure 4a and b, respectively.

The effect of conductive salt concentration on the achieved capacity (Table S2, Supporting Information) is negligible because of the low cycling rate. If the oxidative effect of $NaClO_4$ is causing $(CN)_2$ formation, both electrolytes should result in evolution of a similar magnitude to that shown in Figure 1a for the 1 M $NaClO_4$ electrolyte, however with the reduced concentration of $NaClO_4$ possibly leading to a partial decrease in $(CN)_2$ evolution. It is worth noting that the evolution should not be limited by the available $NaClO_4$. Indeed, in a typical experiment, around 0.25 mmol of CAM is used, but either 0.35 mmol or 0.75 mmol of $NaClO_4$ is contained in the electrolyte, and the CAM does not exhibit substantial degradation according to the voltage profile and capacity. In the case of electrolyte acidity/basicity, a strong difference between the two electrolytes should be observed, as the first has a basicity similar to the initial $NaClO_4$ electrolyte (Figure 1a), while the second should be acidic similar to the initial $NaPF_6$-electrolyte (Figure 1b).

Because the same solvents are used and the water content of electrolyte and PW electrodes is low, the evolution of H_2 and CO_2 reported for both measurements in Figure 4 is similar during charge and overcharge. The release of $(CN)_2$ is observed in both electrolytes, with a pronounced amount detected during overcharge, and with an evolution profile similar to that obtained with a higher concentration of $NaClO_4$, as in Figure 1a. Therefore, the oxidative properties of $NaClO_4$ are confirmed to cause $(CN)_2$ evolution. A difference in peak evolution rates between Figure 1a and 4a is likely due to the dilution of the electrolyte, while the small difference between Figure 4a and 4b may be attributed to a further displacement of ClO_4^- anions in the CEI and electric double layer by PF_6^- anions. This finding also explains the difference in $(CN)_2$ signal intensity observed between previous works in our group (using $NaClO_4$)[48–50] and Geisler's work (using $NaPF_6$).[72] Interestingly, a similar, seemingly contradictory finding at the anode side of SIBs has been also explained by the use of different conductive salts by Goktas *et al.*[65]

Research Article
doi.org/10.1002/batt.202300595
Chemistry Europe
European Chemical Societies Publishing

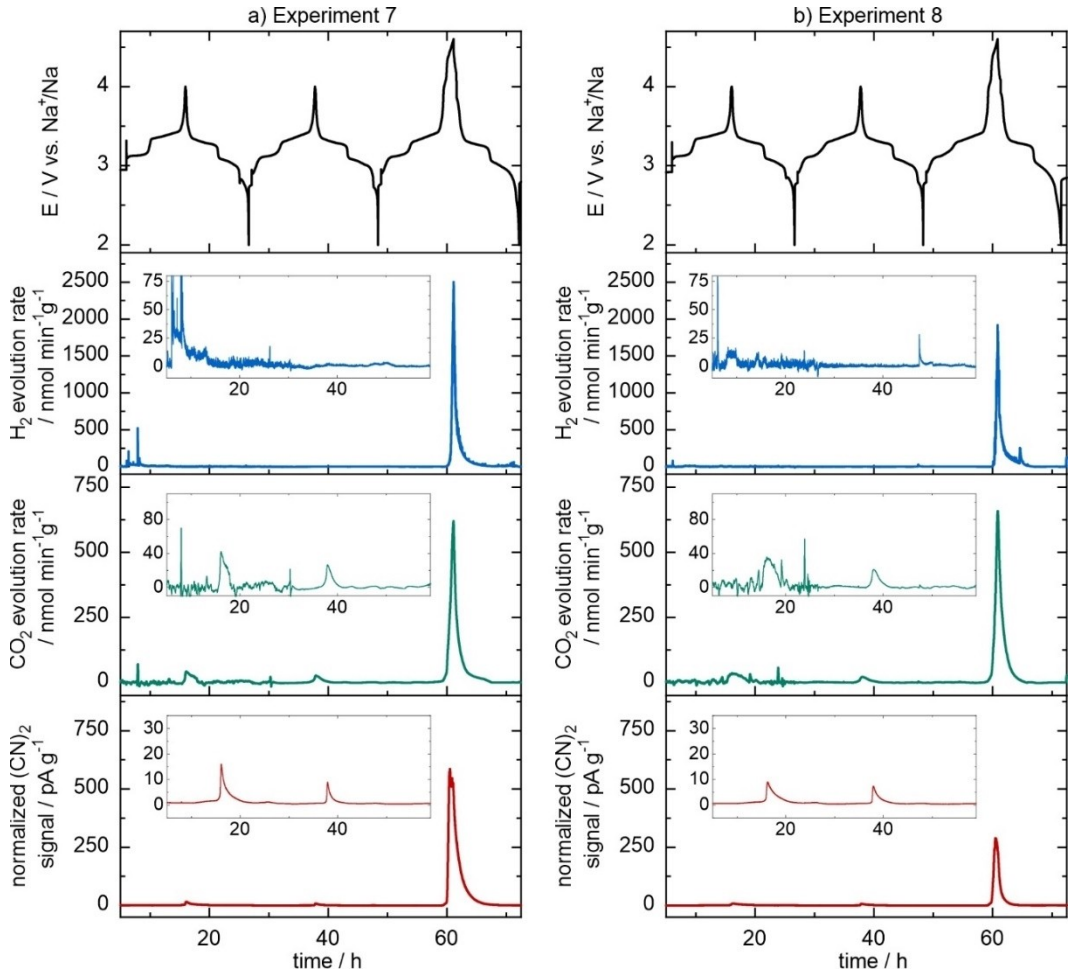

Figure 4. Gas evolution in Na half-cells with a dehydrated PW cathode using EC:PC:DMC = 1:1:1 (v/v/v) with 5 v% FEC as electrolyte solvent and (a) 0.3 M $NaClO_4$ or (b) 0.3 M $NaClO_4$ and 0.7 M $NaPF_6$ as conductive salt.

The detection of $(CN)_2$ evolution in PW-containing cells has significant relevance to the commercial application of PBA/PW cathodes. It is equally relevant to highlight that the cause of $(CN)_2$ evolution is the oxidative nature of the $NaClO_4$ salt, which, while representing a valid model electrolyte salt for laboratory-scale research, cannot be considered a viable option in commercial applications due to its strong oxidation properties and explosive nature in the dry state.[87,98,99] In fact, various novel electrolyte formulations, including alternative conductive salts, such as sodium bis(oxalate)borate, are developed to mitigate safety concerns (to reduce flammability and HF generation, for example) and are already applied to PW CAMs.[47,58,98,100–102]

2.5. Effect of Other Measurement Conditions

Further experiments to evaluate the role of DEMS measurement conditions and trace gas evolution have been carried out and are discussed below. Figure 5a shows the result of a measurement performed at 45 °C instead of 25 °C. Due to increased electrolyte evaporation, a more volatile baseline for H_2 and CO_2 is obtained, with the evolution of these gases being increased both during regular cycling and overcharge. This finding is expected, as electrolyte degradation by hydrolysis and oxidation is increased at elevated temperatures.[83,87] However, the $(CN)_2$ evolution was found to be increased compared to cycling at 25 °C, while it slightly decreased from the 1st to the 2nd charge during regular cycling and then increased during overcharge, but to a much lower extent when compared to the test conducted at 25 °C.

At the same time, the voltage profile of the electrode cycled at 45 °C also strongly deviates after the overcharge, showing a much lower discharge capacity characterized by high irreversibility. Reduced performance of PBA/PW CAMs at elevated temperatures has been reported previously and attributed to degradation and formation of a resistive CEI.[32,45,103] It can be assumed that the formation of such a resistive CEI is not only more severe under overcharge conditions, but that it also prevents further oxidation of the cyanide ions to $(CN)_2$ by restricting charge transfer between ClO_4^- and CAM.

Figure 5b shows the gas evolution from a DEMS measurement conducted with only 350 μL of electrolyte instead of 750 μL. While such a measurement in our setup is more likely to fail due to cell dry-out by carrier gas, it is more realistic in terms

Research Article
doi.org/10.1002/batt.202300595
Chemistry Europe
European Chemical Societies Publishing

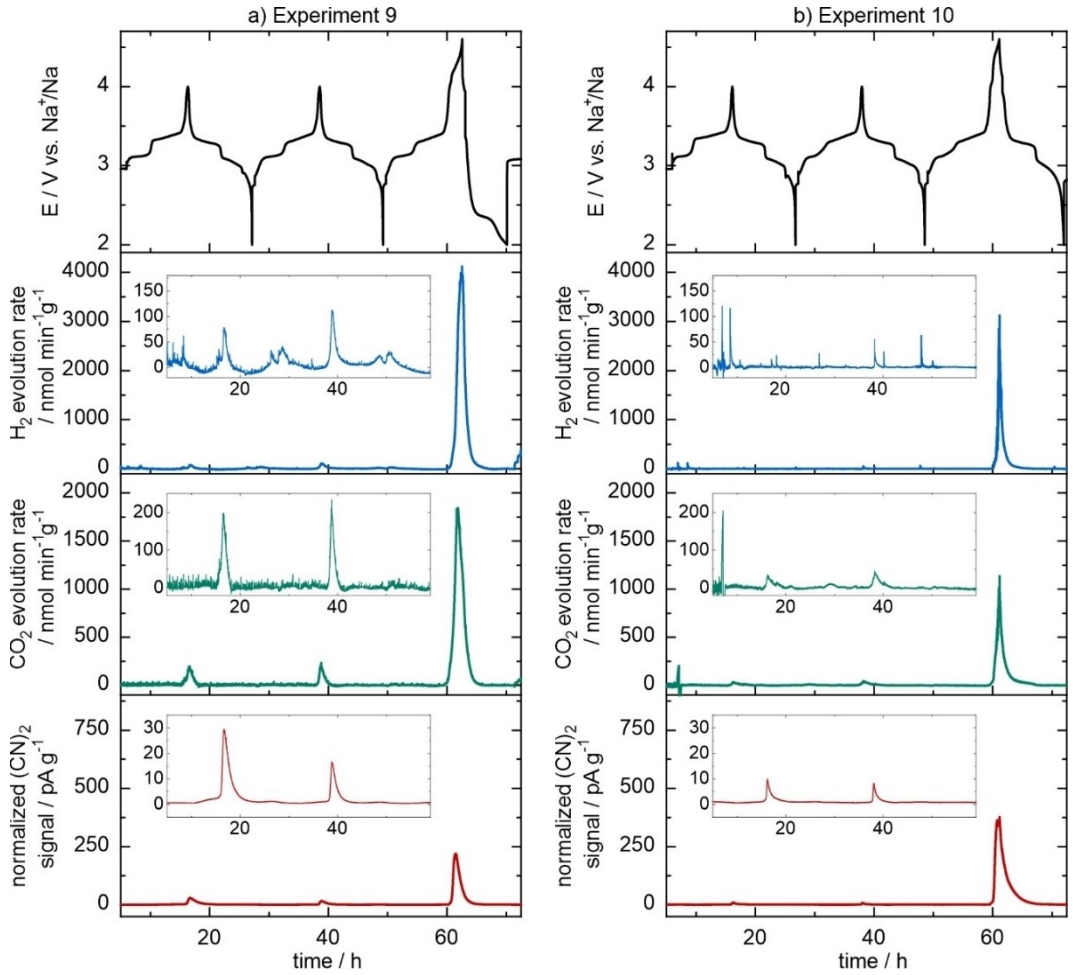

Figure 5. Gas evolution in Na half-cells with a dehydrated PW cathode using 1 M $NaClO_4$ in EC:PC:DMC = 1:1:1 (v/v/v) with 5 v% FEC after (a) increasing temperature from 25 to 45 °C and (b) reducing electrolyte volume from 750 to 350 µL.

of electrolyte to active mass ratio[104] (~5:1 vs. ~12:1, assuming ~1.3 g/mL electrolyte density) and can be more precise due to lower dissolution of gases in the bulk electrolyte, leading to tailing of the evolution curves.[67,105] In this case, no effect on peak tailing is observed and the amounts of H_2 and CO_2 evolved do not differ significantly. Interestingly, the $(CN)_2$ evolution is reduced, yet still significant, especially during overcharge, with a slight peak broadening appearing. A probable explanation is the different absolute amount of $NaClO_4$ in the cell, although a quantitative consumption of $NaClO_4$ is unlikely. Instead, as excess electrolyte is purged out of the cell, the salt concentration is increased in the remaining electrolyte, i.e. that in the glass fiber separator's reservoir, which is less affected by the carrier gas stream. With more initial electrolyte, this effect is more pronounced and leads to a higher effective concentration of $NaClO_4$, similar to the findings of salt concentration variation shown in Figure 4a.

Having established that the lower electrolyte volume does not affect the observed gas evolution beyond the previously discussed differences, lastly, a measurement with this reduced electrolyte volume is carried out without cooling the cold trap of the DEMS setup.[90,91] Since it comes at the price of increased SEM degradation and background noise, as well as reduced target molecule ionization due to electrolyte molecules in the spectrometer, a lower electrolyte volume is necessary to still gather relevant data. This measurement allows to rule out a significant effect of $(CN)_2$ condensation into the cold trap and will also be of interest in the following section on HCN evolution. The resulting gas evolution is shown in Figure S7 (Supporting Information), and as can be seen, none of the gas evolution trends show a significant difference to the measurement with cold trap (Figure 5b). The variation of the peak $(CN)_2$ evolution rate during overcharge appears to be in agreement with the limitations of relative quantification and the observed differences between the experiments combining $NaClO_4$-electrolyte and dehydrated PW electrodes.

2.6. Evolution of Hydrogen Cyanide

Because HCN formation is a side reaction of some PW synthesis routes[22,35,41] and has been previously observed during thermal runaway of PBA cells,[46] and $(CN)_2$ is known to hydrolyze under formation of HCN, in the following, we consider whether HCN is

Research Article
doi.org/10.1002/batt.202300595
Chemistry Europe
European Chemical Societies Publishing

also present during the DEMS measurements. For this, the mass spectrometer's ability to discriminate between molecules of the same gas, but of other isotope composition, referred to as isotopologues, is utilized, which is a powerful enhancement of DEMS study capabilities.[67]

The detection of HCN in the presence of $(CN)_2$ is complicated by fragmentation. At standard conditions (25 °C, 70 eV ionization energy), HCN is detected mostly at $m/z = 27$ (HCN^+, 100% relative intensity) and $m/z = 26$ (CN^+, ~16% relative intensity), as well as in the form of molecules containing a heavier isotope at $m/z = 28$ (~2% relative intensity).[106] $(CN)_2$, on the other hand, is not only detected at $m/z = 52$ (100% relative intensity), but also at $m/z = 26$ (CN^+ fragment and $(CN)_2^{2+}$, ~5% relative intensity) and, due to isotopologues containing either ^{13}C or ^{15}N, at $m/z = 53$ (~3% relative intensity), as well as very weakly in combination of heavy isotope content and fragmentation at $m/z = 27$.[107] In a standard mass spectrometry application, short of gas chromatography, the simultaneous determination of species with overlapping signals, such as HCN and $(CN)_2$, requires solving a set of linear equations obtained with a calibration matrix that contains the fragmentation intensity patterns of all gases of interest.[72,108] In a battery DEMS application, a further difficulty arises from fluctuating background signals, e.g. various $C_2H_x^+$ species from ethylene and DEC fragments ($m/z = 26$, 27, and 28). As background signals are present and no calibration gases and matrix are available, two considerations are presented instead, which allow discussing the relative presence of HCN. In these considerations, three assumptions are made: (1) Molecules other than HCN and $(CN)_2$ contribute only to the baseline, but not to the signal peaks observed for $m/z = 26$, 27, 52, and 53. This is supported by DEMS data of a previous study utilizing the same electrolyte and cutoff potential, but layered oxide CAMs.[109] The respective signal profiles are shown in Figure S8a-c (Supporting Information). (2) The formation rates of $(CN)_2$ isotopologues are similar, i.e. the kinetic isotope effect is weak. (3) There is no significant isotope effect between isotopologues with regards to probabilities of ionization and fragmentation.

Firstly, in all measurements carried out with $NaClO_4$-electrolyte (all DEC-free), $m/z = 27$ peaks can be detected against the background noise, i.e. when the signal noise from excess electrolyte has decreased sufficiently. As evident from Figure 6a-d and S9a-c (Supporting Information), the peak raw signal of $m/z = 27$ is detected between 2.9 and 9.8 min earlier than that of $(CN)_2$ at $m/z = 26$ and 52 in some measurements. However, each mass channel is scanned every 13.5 s for the experiments in this study, resulting in a 13 to 43 scan cycle difference between peak signal rates. In Figure 6d, instead of an earlier peak signal, a stronger peak shoulder is observed for $m/z = 27$. However, as shown in Figure S9a (Supporting Information), the effect is reversed in the case of simultaneous presence of $NaClO_4$ and $NaPF_6$.

If fragmentation were the sole source of signal beyond background in all three of these channels, peak signal rates would occur figuratively simultaneously, as they have a common source in the $(CN)_2$ molecule, which is only ionized and fragmented in the mass spectrometer. The time between ionization at the ion source and detection at the SEM is extremely short compared to the duration of the experiment and even the length of one scan cycle. The fact that the $m/z = 27$ signal peak occurs much earlier suggests that, additionally to the $^{13}C^{14}N^+$ or $^{12}C^{15}N^+$ fragment of $(CN)_2$, another gas (in this case, HCN) contributes to the overall signal, which is either formed slightly earlier or transported to the spectrometer faster.

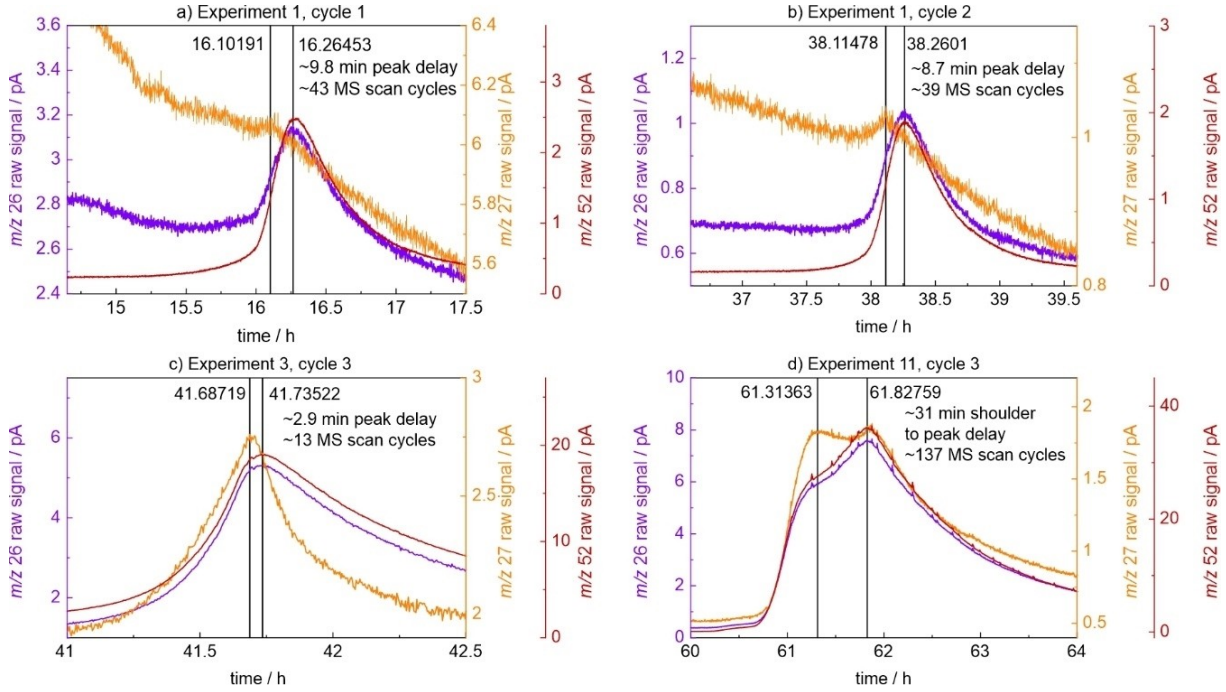

Figure 6. Delay in signal peaks between m/z = 26 and m/z = 27 and 52 indicating the presence of trace amounts of HCN.

Research Article
doi.org/10.1002/batt.202300595
Chemistry Europe
European Chemical Societies Publishing

Assuming laminar flow of carrier gas, a slightly earlier peak formation rate of HCN in the cell may be assumed. However, from the low signal-to-noise ratio in $m/z=27$, a low concentration of HCN can be inferred. Another limitation that should be considered is the reactivity of $(CN)_2$, both in the presence of traces of moisture and H_2. The earlier peak formation rate is not necessarily found in the cell, but can occur in the DEMS tubing by hydrolysis or reduction of $(CN)_2$, similar to the detection of PF_5 as POF_3, as reported by Solchenbach *et al.*[81] A similar HCN formation reaction, albeit not affecting peak evolution rate time differences, is reduction of $(CN)_2$ in the presence of H_2 at the hot filament of the mass spectrometer, a reaction known to occur under these conditions between Cl_2 and H_2.[110] Secondly, one may consider isotope abundance and relative intensity ratios. At this point, it should be noted that while both for National Institute of Standards and Technology (NIST) reference data[106,107] and for the DEMS measurements an ionization energy of 70 eV was applied, yet a slight deviation of relative intensities can be observed due to different temperatures during ionization.[81,87]

Under the previously made assumptions, in the case of pure $(CN)_2$, the peak intensity ratio (1) between $m/z=26$ and 52, on the one hand, and $m/z=53$ and 52, on the other hand, should be close to the NIST reference values of 4.7 and 3.1%, respectively,[107] and (2) between $m/z=27$ and 26 should be around half that between $m/z=53$ ("heavy $(CN)_2$") and 52. Since only one of the two fragments of "heavy $(CN)_2$" carries a heavy isotope, single ionization followed by fragmentation leads to only one of the two fragments carrying the charge. Additionally, the $m/z=26$ signal may also be increased from traces of $(CN)_2^{2+}$. However, if an increasing concentration of HCN is present, both the $m/z=26$ and 27 signals are increased, with the latter increasing almost 6 times more, as in pure HCN the ratio between $m/z=26$ and 27 is ~17%.[106] A deviation of the ratios discussed above can therefore indicate the presence of HCN.

As shown in Figure 7a-c and Figure S10a-c and Table S6 (Supporting Information), the intensity of all four raw signal peaks is determined and compared for a series of measurements. The ratio between $m/z=53$ and 52 was found to be between 2.5 and 2.9%, close to the NIST reference value of 3.1%.[107] However, the ratio between $m/z=26$ and 52 was found to be between 20.3 and 24.2% in the measurements, far above the NIST reference value of 4.7%. A stronger relative signal of $m/z=27$ is then also found for the ratio between $m/z=27$ and 26, between 12.2 and 20%. While a linear equation system could be solved for the shares of HCN and $(CN)_2$ that generate these relative intensities, the result would be the share of ionized molecules. The latter differs significantly from the actual share of molecules due to different electron ionization cross sections between HCN and $(CN)_2$, so that again a calibration gas containing known quantities of both gases would be needed for a precise determination, even of ratios.[72,108,111] If, for a rough estimation, the ionization probability of both gases is assumed to be equal and all $m/z=27$ signal is attributed to HCN, the ratio between $m/z=27$ and 52 would indicate additional HCN evolution in the range of 2.9 to 4.8% of the $(CN)_2$ evolution. No major differences in the observed ratios between the measurements (see Table S6, Supporting Information) further demonstrate that neither water content nor electrolyte volume or cold-trap settings significantly affect the perceived ratio between HCN and $(CN)_2$.

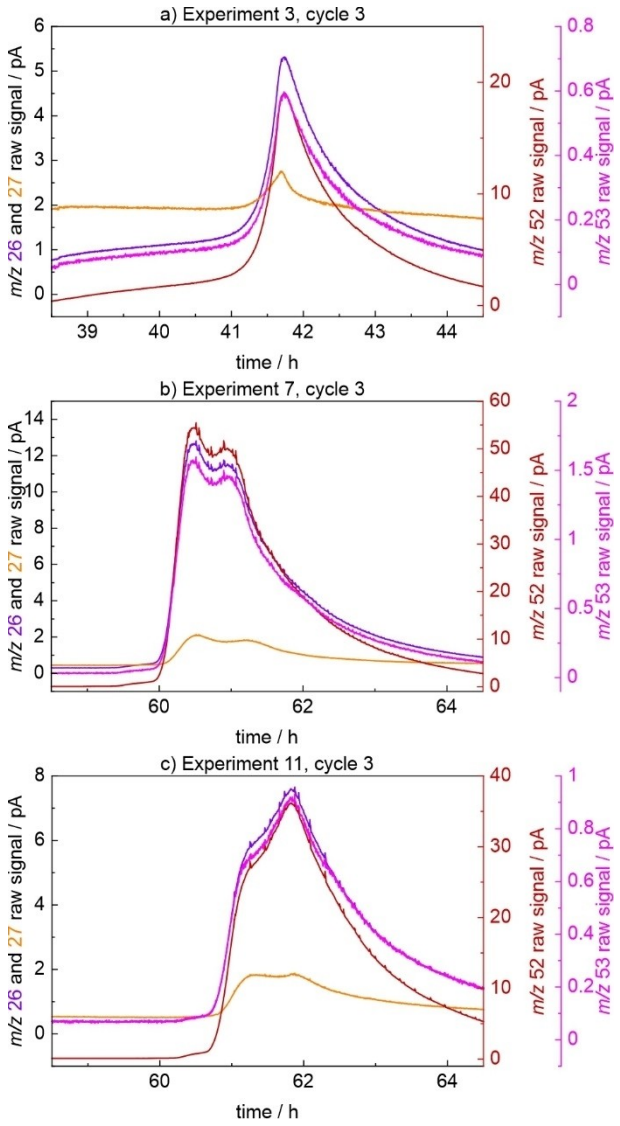

Figure 7. Ratios of m/z = 26, 27, 52, and 53 raw signal intensities indicating the formation of trace amounts of HCN, as m/z = 27 signal is stronger than expected for a mere isotopologue fragment.

2.7. Mechanistic Considerations and Discussion

In light of the results presented so far and the available literature, a consideration of likely gas amount and formation mechanism of $(CN)_2$ shall be discussed. In the initially reported observation of $(CN)_2$ evolution, a comparison was made to the release of lattice oxygen from layered oxide CAMs, another anion oxidation process.[48] Having found $NaClO_4$ to play a significant role in the $(CN)_2$ formation, this now has to be reconsidered, also taking into account a difference in reversi-

bility. Between O^{2-} ions and oxygen gas, peroxides and hyperoxide anions exist, allowing for an often at least partially reversible, capacity providing anion redox.[112,113] While a respective $(CN)_2^-$ anion has been discussed in the literature, this discussion is limited to theoretical calculations of anions in the atmosphere of Saturn's moon Titan.[114,115] The presence of this species in PW CAM therefore appears unlikely, so that cyanide oxidation is irreversible. Still, some similarities between the loss of O_2 from layered oxides and $(CN)_2$ from PW may exist. In layered oxides, an oxygen-depleted surface forms, commonly referred to as rocksalt-type phase. This layer impedes ion diffusion (the transition metals in it become redox inactive) and with its thickness increasing during cycle life, helps explain some of the capacity fading seen in layered oxide CAMs.[116] In the case of rocksalt-type layer, a measurement of the evolved gases can be used to calculate the fraction of CAM converted to oxygen-depleted material and, taking the specific surface area of the CAM particles into account, layer thickness, with a conversion of ~2% being reported for strong overcharge conditions.[117,118]

A similar, cyanide-depleted surface may form on the PW particles, as contact to $NaClO_4$ and gas diffusion into the electrolyte are only possible at the particle surface. While its detection via transmission electron microscopy (TEM) proves troublesome due to the susceptibility of hexacyanoferrates to beam damage, Yan *et al.* reported X-ray photoelectron spectroscopy (XPS) and Fourier-transform infrared spectroscopy (FTIR) findings of a cycled PBA cathode that indicate the formation of an altered surface layer or CEI when using $NaPF_6$-electrolyte.[45] Interestingly, Sottmann *et al.* observed the formation of $NaMnCl_3$ via X-ray diffraction (XRD) of a cycled manganese hexacyanoferrate cathode, with a reduction of $NaClO_4$ as the only possible source of Cl^- anions.[56] A reaction of no more than 1 to 2% of PBA/PW CAM seems probable. Firstly, as also reported by Sottmann *et al.*[56] and Piernas-Muñoz *et al.*,[60] a change of conductive salt to $NaPF_6$ does not lead to a substantial increase in capacity retention, ruling out a noticeably stronger decomposition of the CAM by $NaClO_4$. Furthermore, long-term cycling of PBA/PW CAM is still possible in $NaClO_4$-electrolyte, suggesting that the degradation reaction is limited in its extent. Thus, a likely reason is the limitation of the reaction to the available particle surface.

However, the calculation of how much $(CN)_2$ is evolved requires the number of reacting cyanide ions per formula unit of degrading hexacyanoferrate to be known. A full conversion (3 molecules of $(CN)_2$ per $Fe[Fe(CN)_6]$ unit) would yield iron oxides, hydroxides or chlorides, in agreement with the observation of $NaMnCl_3$ formation by Sottmann *et al.*,[56] yet through a series of intermediate species of unknown reactivity. Alternatively, only one or two cyanide ligands per hexacyanoferrate unit may be oxidized, further reducing the estimated amount of $(CN)_2$ evolution by a factor of 1/6 or 1/3. Cheah *et al.* reported $(CN)_2$ evolution due to an irreversible electrochemical oxidation of hexacyanoferrate at 0.586 V vs. Fc^+/Fc in acetonitrile.[119] Interestingly, this potential corresponds to ~3.93 V vs. Na^+/Na [$E^0(Fc^+/Fc) = 0.63$ V vs. SHE,[120] $E^0(Na^+/Na) = 2.714$ V vs. SHE], close to the onset of $(CN)_2$ evolution observed in this work. Cheah *et al.* proposed an ECE-type reaction, involving both electron transfer and chemical reaction steps, in which the electrochemical formation of an Fe^{4+} intermediate is followed by $(CN)_2$ release in a reductive elimination reaction of two cyanide ligands, and the resulting Fe^{2+} complex is subsequently electrochemically oxidized to Fe^{3+}. The solvent then coordinates the iron in place of the missing cyanide ligands, which Cheah *et al.* demonstrated via *in-situ* FTIR and X-ray absorption spectroscopy (XAS) in combination with density-functional theory (DFT) calculations.[119] For the PBA/PW CAM discussed here, a coordination is similarly possible by electrolyte solvent, water or hydroxide anions. The findings of Cheah *et al.* are significant for the interpretation of results in this study in multiple ways. Most importantly, they explain why a lower $(CN)_2$ evolution is observed also in cells containing $NaPF_6$-electrolyte, since Fe^{4+} may be formed both electrochemically (to a lesser extent, but in all electrolytes) and via oxidation by $NaClO_4$ (to a greater extent). Consequently, this means that electron transfer occurs between Fe^{3+} and ClO_4^- or a ClO_x species formed by decomposition of the latter and does not immediately involve the cyanide anions. This, in turn, helps to explain the otherwise contrary findings of Pan *et al.*, who reported on gas-free oxidation of NaCN/carbon electrodes in $NaClO_4$-electrolyte for sodium-ion capacitors, finding polycyanogen (also called paracyanogen) instead of $(CN)_2$ gas, as supported by pressure measurements (and DEMS, but without explicitly monitoring $m/z = 52$).[121] Polycyanogen formation was then demonstrated by elemental analysis, as well as by ultraviolet (UV)- and IR-spectroscopy, and assumed to occur due to anionic polymerization in the presence of cyanide anions.[121,122] Guo *et al.* studied the electrochemical oxidation of cyanide in acetonitrile by electrospray-mass spectrometry (ES-MS) and similarly reported nucleophilic addition of cyanide to cyanogen, observing various $(CN)_n$ oligomers, but no $(CN)_2$.[123]

An attempt was made by us to conduct DEMS measurements on NaCN/carbon composite electrodes similar to those of Pan *et al.*,[121] with the further intent, similar to the Li_2CO_3 decomposition study of Freiberg *et al.*,[85] to also quantify the consumed NaCN and thereby $(CN)_2$ amounts. However, this proved unsuccessful, as with the only available PVDF binder, slurry gelation was observed upon the presence of NaCN. Since PVDF slurry gelation occurs by dehydrofluorination,[124] the formed HF likely reacts with NaCN to form HCN. This not only invalidates quantification, but also poses a significant safety risk, and no further attempts were made to prepare NaCN electrodes.

In this study, polycyanogen formation could be neither proved nor disproved. Still, taking the literature findings detailed above into consideration, some characteristics of $(CN)_2$ formation and evolution can be discussed. The $(CN)_2$ formation via reductive elimination in an Fe^{4+} complex explains why the oxidation of cyanide, in at least some cases, ends already at $(CN)_2$ and does not carry on to cyanate ions. Furthermore, the relative absence of free cyanide anions inhibits the anionic polymerization to polycyanogen by nucleophilic addition. The anions present in the electrolyte are far less nucleophilic, with the notable exception of hydroxide anions. The reduced $(CN)_2$

evolution observed in the case of overcharge of undried electrodes and $NaClO_4$ (Figure 2a) may then also be partially attributed to the addition of hydroxide to formed $(CN)_2$, yielding 1-cyanoformamide instead.[125] At the same time, the presence of water under acidic conditions (Figure 3b) may not lead to $(CN)_2$ polymerization, and may also induce formation of reactive oxygen species upon electrochemical water oxidation, in both cases explaining the higher $(CN)_2$ evolution observed in this measurement.

For the reductive elimination reaction, a preceding dissolution of one cyanide ligand to form a more reactive, five-coordinate intermediate cannot be ruled out and may explain the observed $m/z = 27$ signals and their earlier peak evolution rate.[126] While Fe^{4+} is unusual and its presence in a hexacyanoferrate complex, as proposed by Cheah *et al.*,[119] is likely too short-lived to be detected, it has been previously reported both as an electrochemically formed intermediate prone to reductive elimination in organometallic chemistry[127] and in battery materials, often showing spontaneous reduction at high SOC as part of a reductive coupling mechanism, leading to oxidized anions.[128–132]

Lastly, the fate of the ClO_4^- anion shall be considered. Eggert *et al.* studied the gas evolution of $LiClO_4$ in PC on Pt electrodes and proposed a single electron-transfer reaction, yielding a $ClO_4^{\bullet}$ radical, which decomposes to ClO_2 and oxygen. The oxygen then contributes to electrolyte oxidation, leaving both ClO_2 ($m/z = 67$, $m/z = 69$ due to ^{35}Cl and ^{37}Cl) and CO_2 as detected gases.[133] Cattaneo *et al.* also reported ClO_2 evolution of this electrolyte on acetylene black electrodes above 4.5 V vs. Li^+/Li.[134] On the other hand, Metzger *et al.* did not observe any ClO_2 signals in their study of conductive carbon oxidation by $LiClO_4$ and additionally ruled out the formation of LiCl via XPS, thus assuming $LiClO_x$ species as the reaction product.[87] However, Sottmann *et al.* reported the formation of $NaMnCl_3$, which does contain the Cl^- anion.[56] As is shown in Figure S11a-e (Supporting Information), in this work, under overcharge conditions and especially at increased temperature, signals at $m/z = 67$, 69, and 51 ($^{35}ClO^+$, $m/z = 53$ occupied by $(CN)_2$ isotopologue) are observed, mirroring the correct isotope ratio of ^{35}Cl and ^{37}Cl. No clear signal could be made out for $m/z = 35$ and 37. However, due to the strong level of background noise and possible other contributions, the finding can only be considered with caution. Furthermore, the formation of a $ClO_4^{\bullet}$ radical itself is not proven, and it is an oxidation (not the reduction) required to facilitate the Fe^{3+} to Fe^{4+} electron removal. For this, either the reverse reaction, or more likely oxidation by a formed decomposition species (ClO_x), itself an oxidative radical, is required. This is supported by the lack of ClO_2 signals in previous measurements with the same electrolyte on layered oxide CAMs (Figure S8, Supporting Information), indicating that ClO_2 is only formed together with PW degradation and not itself causing the degradation.

Taken together, a plausible reductive elimination mechanism for the formation of $(CN)_2$ and the observed formation of ClO_2 from $NaClO_4$ suggests that a reactive ClO_x species facilitates the formation of a Fe^{4+} intermediate.

3. Conclusions

In this work, we have shown (quantitatively) that the outgassing of PW materials is dominated by the evolution of H_2, especially in hydrated CAM and especially during overcharge (4.6 V). CO_2 evolution during regular cycling occurs from the hydrolysis of organic carbonates by hydroxide anions and therefore depends not only on the water content of the CAM, but also on the conductive salt, as $NaPF_6$ hydrolysis leads to acidic conditions (less hydrolysis), while $NaClO_4$ leads to basic conditions (more hydrolysis). Only under overcharge conditions at higher potentials, electrochemical oxidation of electrolyte with CO_2 release occurs. In addition, the evolution of $(CN)_2$ was investigated in detail in this study, indicating that significant $(CN)_2$ release stems from the use of oxidative $NaClO_4$, while $(CN)_2$ release from electrolyte with $NaPF_6$ is much lower. With further experiments, other influence factors and the evolution of HCN were discussed, finding that HCN is likely present in traces, but due to the higher concentration of $(CN)_2$, the latter dominates in terms of safety risks. A hypothesis regarding the formation mechanism and quantity of $(CN)_2$ is presented, centering on the formation of a reactive, cyanide-coordinated Fe^{4+} intermediate that undergoes reductive elimination.

4. Outlook

$(CN)_2$ evolution during cycling of PW-based SIBs has severe implications regarding not only safety and handling of the materials and cells, but also their commercial application. However, we would like to emphasize that it is the commercially irrelevant $NaClO_4$ salt – often used in lab-scale studies – that mainly causes the $(CN)_2$ evolution. Furthermore, as also shown in this study, H_2 evolved due to PW water content is the predominant gas and comes with its own safety risks. The implied further development needs for PW-based SIBs are therefore, on the one hand, safer electrolytes and conductive salts and, on the other hand, careful and controlled dehydration procedures while maintaining high sodium content, especially when using aqueous processed electrodes.

Lastly, some important experimental considerations represent the limitations of the DEMS setup employed here. Reported potentials are determined against Na metal acting both as counter and reference electrode, which may have been affected by the formation of a resistive SEI. While it was shown that the use of a cold trap did not lead to substantial amounts of HCN or $(CN)_2$ being condensed, the evolved $(CN)_2$ was continually extracted, whereas in a regular cell, it would remain in the headspace and also partially be dissolved into the electrolyte. Under these conditions, polymerization to polycyanogen or follow-up reactions, such as with the H_2 or electrolyte solvent, may occur, forming HCN or organic nitrile species, and change the outcome of gas evolution studies performed on a closed headspace, such as crimped-capillary online electrochemical mass spectrometry (OEMS) or GC-MS headspace sampling.[66,104,135] On a similar note, if $(CN)_2$ evolution occurs in aqueous electrolyte,[16] often $NaClO_4$ based, it would be

followed up by hydrolysis, yielding cyanate and cyanide ions, of which the latter may be oxidized again, leaving cyanate ions as the main degradation product instead of $(CN)_2$. Therefore, additional experiments are still required to evaluate the significance of $(CN)_2$ evolution for the application of PBAs/PWs as battery materials. This includes experiments in full cells and with a reference electrode,[72,136] experiments where a correct electrolyte-to-active material ratio limits the amount of conductive salt and electrolyte available for degradation reactions, i.e. measurements in larger cell formats,[137,138] and a reliable and precise quantification and separation of both HCN and $(CN)_2$, which may be achieved by novel DEMS cell designs, such as on-chip electrochemistry-mass spectrometry (EC-MS).[139]

To better understand follow-up reactions, we envision that labeling the PW CAM with ^{13}CN may allow for the detection of gaseous products via DEMS/OEMS and electrolyte side products via ^{13}C nuclear magnetic resonance (NMR) spectroscopy. Overall, the findings highlight the importance of gas evolution measurements for an exhaustive characterization of battery materials, and the effect of coating, doping, additives, synthesis, and processing procedures on suppression of $(CN)_2$ evolution may become a new field of consideration in PBA/PW research.

Experimental Section

Electrodes based on PW CAM with a nominal composition of $Na_{1.80(5)}Fe[Fe(CN)_6]\cdot 1.84(3)H_2O$ were prepared as described previously.[43] In short, an aqueous slurry was produced from PW, carboxymethyl cellulose (CMC) and styrene-butadiene rubber (SBR) binder, and conductive carbon additive in a weight ratio of 93.5 : 3.5 : 3.0. After degassing, the slurry was coated onto a 15 μm aluminium foil (Avotec Steel). Electrodes were calendared to a targeted density of ~1.5 $g\,cm^{-3}$, with an average mass loading of 13 (±1) $mg\,cm^{-2}$. Electrode disks of 30 mm diameter were punched out and dried under a dynamic vacuum for 24 h at 170 °C using a Glass Oven b-585 (BUCHI UK Ltd) to allow for dehydration of the Na-rich hydrated PW system. Undried electrodes were also used in this work to investigate the effect of interstitial and adsorbed water on gas evolution upon cycling.[43]

For DEMS measurements, a customized cell was assembled using a Na-metal (BASF SE) counter electrode, a GF/D separator (Whatman), and the 30 mm PW cathode as working electrode, with an additional 4 mm diameter hole punched out in the center to allow for gas flow. 750 μL of electrolyte was spread out on the separator dropwise. Different electrolyte systems were used in the work, including 1 M $NaPF_6$ in a mixture of ethylene carbonate (EC) and diethyl carbonate (DEC) in a ratio of 3 : 7 (v/v) (Fluorochem Ltd.) and 0.3 or 1 M $NaClO_4$ (Sigma-Aldrich), 1 M $NaPF_6$ or 0.3 M $NaClO_4$ and 0.7 M $NaPF_6$ in a mixture of EC, propylene carbonate (PC, Merck KGaA), and dimethyl carbonate (DMC, BASF SE) in a ratio of 1 : 1 : 1 (v/v/v) containing an additional 5 v% of fluoroethylene carbonate (FEC, BASF SE). Cells were cycled galvanostatically at 14 $mA\,g^{-1}$ (1 C = 140 $mA\,g^{-1}$) for two cycles within a standard potential range between 2.0 and 4.0 V vs. Na^+/Na, and then charged up to 4.6 V before being discharged to 2.0 V in the third cycle. A constant stream of He carrier gas (2.5 mL min^{-1}, purity 6.0) was passed through the cell during cycling, and the extracted gas mixture then passed through a cold trap (−8 °C) before being analyzed by a mass spectrometer (GSD320, Pfeiffer Vacuum GmbH). A more detailed description of the DEMS setup and measurement principle can be found in the literature.[67,90,91] A baseline correction is applied to the $m/z = 2$, 26, and 44 signals to subtract the background signal stemming from electrolyte solvent molecules, residual air, and cell leakage. Calibration curves for H_2 ($m/z = 2$) and CO_2 ($m/z = 44$) were obtained by subsequently passing a calibration gas with known concentrations of these species in He through the cell in various dilutions. This is demonstrated for the first four measurements in Figure S2 (Supporting Information). The secondary electron multiplier (SEM) voltage was adjusted before each measurement in a range of 1200–1380 V to obtain a He ($m/z = 4$) raw signal close to 10^{-7} A. To compensate for differences in SEM gain and electrode loading, the $(CN)_2$ raw signal ($m/z = 52$) was normalized to CAM weight and relative H_2/CO_2 calibration curve slopes, as discussed in the main text. To this end, the quotients between each slope and the average slope of the first four measurements were calculated for both H_2 and CO_2, then averaged and the $m/z = 52$ raw signal divided by this value.[50] Table S3 (Supporting Information) contains the H_2 and CO_2 calibration slopes and resulting adjustment factors for all measurements.

Acknowledgements

The authors thank Yanjiao Ma (KIT, now Nanjing Normal University) for providing the high-entropy PW materials that initially started this research project as well as $NaClO_4$-electrolyte and Na metal. Leonhard Karger (KIT) is acknowledged for insightful mechanistic considerations. This study was partially supported by BASF SE. J. J. acknowledges funding and discussion within the POLiS Cluster of Excellence (ID 390874152, DFG – German Research Foundation). I. H. and F. M. M. acknowledge funding received from the European Union's Horizon 2020 research and innovation programme under grant agreement no. 883753 (SIMBA – Sodium-Ion and Sodium Metal Batteries for Efficient and Sustainable Next-Generation Energy Storage). I. H. acknowledges also funding received by the Royal Society through Research Grant RGS\R1\231519 "Gas Evolution Monitoring in Na-Ion Batteries (GEMINI)". Open Access funding enabled and organized by Projekt DEAL.

Conflict of Interests

The authors declare no conflict of interests.

Data Availability Statement

The data that support the findings of this study are available from the corresponding author upon reasonable request.

Keywords: Prussian white cathode · sodium-ion battery · gas evolution · cyanogen · hydrogen cyanide

[1] Z. Zhu, T. Jiang, M. Ali, Y. Meng, Y. Jin, Y. Cui, W. Chen, *Chem. Rev.* **2022**, *122*, 16610–16751.
[2] A. Masias, J. Marcicki, W. A. Paxton, *ACS Energy Lett.* **2021**, *6*, 621–630.
[3] D. Karabelli, S. Kiemel, S. Singh, J. Koller, S. Ehrenberger, R. Miehe, M. Weeber, K. P. Birke, *Front. Energy Res.* **2020**, *8*, 594857.

[4] C. Xu, Q. Dai, L. Gaines, M. Hu, A. Tukker, B. Steubing, *Commun. Mater.* **2020**, *1*, 99.
[5] J. M. Tarascon, *Joule* **2020**, *4*, 1616–1620.
[6] T. Yu, G. Li, Y. Dian, Y. Wu, T. Zhang, X. Zhao, M. Luo, Y. Liu, *J. Alloys Compd.* **2023**, *958*, 170486.
[7] L. Zhao, T. Zhang, W. Li, T. Li, L. Zhang, X. Zhang, Z. Wang, *Engineering* **2023**, *24*, 172–183.
[8] Y. Tian, G. Zeng, A. Rutt, T. Shi, H. Kim, J. Wang, J. Koettgen, Y. Sun, B. Ouyang, T. Chen, Z. Lun, Z. Rong, K. Persson, G. Ceder, *Chem. Rev.* **2021**, *121*, 1623–1669.
[9] Q. Liu, Z. Hu, M. Chen, C. Zou, H. Jin, S. Wang, S. L. Chou, Y. Liu, S. X. Dou, *Adv. Funct. Mater.* **2020**, *30*, 1909530.
[10] H. S. Hirsh, Y. Li, D. H. S. Tan, M. Zhang, E. Zhao, Y. S. Meng, *Adv. Energy Mater.* **2020**, *10*, 2001274.
[11] I. Hasa, S. Mariyappan, D. Saurel, P. Adelhelm, A. Y. Koposov, C. Masquelier, L. Croguennec, M. Casas-Cabanas, *J. Power Sources* **2021**, *482*, 228872.
[12] M. Baumann, M. Häringer, M. Schmidt, L. Schneider, J. F. Peters, W. Bauer, J. R. Binder, M. Weil, *Adv. Energy Mater.* **2022**, *12*, 2202636.
[13] A. N. Singh, M. Islam, A. Meena, M. Faizan, D. Han, C. Bathula, A. Hajibabaei, R. Anand, K.-W. Nam, *Adv. Funct. Mater.* **2023**, *33*, 2304617.
[14] J. Qian, C. Wu, Y. Cao, Z. Ma, Y. Huang, X. Ai, H. Yang, *Adv. Energy Mater.* **2018**, *8*, 1702619.
[15] J. Peng, W. Zhang, Q. Liu, J. Wang, S. Chou, H. Liu, S. Dou, *Adv. Mater.* **2022**, *34*, 2108384.
[16] M. Jiang, Z. Hou, L. Ren, Y. Zhang, J. G. Wang, *Energy Storage Mater.* **2022**, *50*, 618–640.
[17] K. Hurlbutt, S. Wheeler, I. Capone, M. Pasta, *Joule* **2018**, *2*, 1950–1960.
[18] H. Jiaqi, R. Du, H. Zhang, Y. Liu, C. Jian, Y. Liu, L. Li, J. Peng, Y. Qiao, S. Chou, *Chem. Commun.* **2023**, *2*, 9320–9335.
[19] I. Hasa, N. Tapia-Ruiz, M. Galceran, *Front. Energy Res.* **2022**, *10*, 1076764.
[20] I. Hasa, J. Barker, G. Elia, S. Passerini, *Sodium Systems | Low Temperature: Overview, in: Reference Module in Chemistry, Molecular Sciences and Chemical Engineering*, **2023**, Elsevier: Amsterdam (DOI: 10.1016/B978-0-323-96022-9.00061-X).
[21] L. Hartmann, J. Deshmukh, L. Zhang, S. Buechele, M. Metzger, *J. Electrochem. Soc.* **2023**, *170*, 030540.
[22] D. O. Ojwang, M. Svensson, C. Njel, R. Mogensen, A. S. Menon, T. Ericsson, L. Häggström, J. Maibach, W. R. Brant, *ACS Appl. Mater. Interfaces* **2021**, *13*, 10054–10063.
[23] D. O. Ojwang, L. Häggström, T. Ericsson, R. Mogensen, W. R. Brant, *Dalton Trans.* **2022**, *51*, 14712–14720.
[24] W. Wang, Y. Gang, J. Peng, Z. Hu, Z. Yan, W. Lai, Y. Zhu, D. Appadoo, M. Ye, Y. Cao, Q.-F. Gu, H.-K. Liu, S.-X. Dou, S.-L. Chou, *Adv. Funct. Mater.* **2022**, *32*, 2111727.
[25] Y. Ma, Y. Hu, Y. Pramudya, T. Diemant, Q. Wang, D. Goonetilleke, Y. Tang, B. Zhou, H. Hahn, W. Wenzel, M. Fichtner, Y. Ma, B. Breitung, T. Brezesinski, *Adv. Funct. Mater.* **2022**, *32*, 2202372.
[26] Y. Xi, Y. Lu, *ACS Appl. Mater. Interfaces* **2022**, *14*, 39022–39030.
[27] Y. Huang, X. Zhang, L. Ji, L. Wang, B. Bin Xu, M. W. Shahzad, Y. Tang, Y. Zhu, M. Yan, G. Sun, Y. Jiang, *Energy Storage Mater.* **2023**, *58*, 1–8.
[28] Y. You, X. L. Wu, Y. X. Yin, Y. G. Guo, *Energy Environ. Sci.* **2014**, *7*, 1643–1647.
[29] J. Peng, Y. Gao, H. Zhang, Z. Liu, W. Zhang, L. Li, Y. Qiao, W. Yang, J. Wang, S. Dou, S. Chou, *Angew. Chem. Int. Ed.* **2022**, *61*, e202205867.
[30] J. Peng, W. Zhang, Z. Hu, L. Zhao, C. Wu, G. Peleckis, Q. Gu, J. Z. Wang, H. K. Liu, S. X. Dou, S. Chou, *Nano Lett.* **2022**, *22*, 1302–1310.
[31] J. Peng, M. Ou, H. Yi, X. Sun, Y. Zhang, B. Zhang, Y. Ding, F. Wang, S. Gu, C. A. López, W. Zhang, Y. Liu, J. Fang, P. Wei, Y. Li, L. Miao, J. Jiang, C. Fang, Q. Li, M. T. Fernández-Díaz, J. A. Alonso, S. Chou, J. Han, *Energy Environ. Sci.* **2021**, *14*, 3130–3140.
[32] X. Huang, C. Yang, Y. You, *ACS Appl. Energ. Mater.* **2022**, *5*, 8123–8131.
[33] Y. Yang, E. Liu, X. Yan, C. Ma, W. Wen, X.-Z. Liao, Z.-F. Ma, *J. Electrochem. Soc.* **2016**, *163*, A2117–A2123.
[34] S. Wang, M. Qin, M. Huang, X. Huang, Q. Li, Y. You, *ACS Appl. Energ. Mater.* **2022**, *5*, 6927–6935.
[35] W. R. Brant, R. Mogensen, S. Colbin, D. O. Ojwang, S. Schmid, L. Häggström, T. Ericsson, A. Jaworski, A. J. Pell, R. Younesi, *Chem. Mater.* **2019**, *31*, 7203–7211.
[36] L. Shen, Y. Jiang, Y. Jiang, J. Ma, K. Yang, H. Ma, Q. Liu, N. Zhu, *ACS Appl. Mater. Interfaces* **2022**, *14*, 24332–24340.
[37] J. Peng, J. Huang, Y. Gao, Y. Qiao, H. Dong, Y. Liu, L. Li, J. Wang, S. Dou, S. Chou, *Small* **2023**, 2300435.
[38] Y. Liu, S. Fan, Y. Gao, Y. Liu, H. Zhang, J. Chen, X. Chen, J. Huang, X. Liu, L. Li, Y. Qiao, S. Chou, *Small* **2023**, 2302687.
[39] P. Wang, Y. Li, D. Zhu, F. Gong, S. Fang, Y. Zhang, S. Sun, *Dalton Trans.* **2022**, *51*, 9622–9626.
[40] M. Li, M. Gaboardi, A. Mullaliu, M. Maisuradze, X. Xue, G. Aquilanti, J. R. Plaisier, S. Passerini, M. Giorgetti, *ChemSusChem* **2023**, *16*, e202300201.
[41] X. H. Liu, J. Peng, W. H. Lai, Y. Gao, H. Zhang, L. Li, Y. Qiao, S. L. Chou, *Adv. Funct. Mater.* **2022**, *32*, 2108616.
[42] X. M. Lin, X. T. Yang, H. N. Chen, Y. L. Deng, W. H. Chen, J. C. Dong, Y. M. Wei, J. F. Li, *J. Energy Chem.* **2023**, *76*, 146–164.
[43] F. Maddar, D. Walker, T. W. Chamberlain, J. Compton, A. S. Menon, M. Copley, I. Hasa, *J. Mater. Chem. A* **2023**, *11*, 15778–15791.
[44] S. Gourang Patnaik, I. Escher, G. A. Ferrero, P. Adelhelm, *Batteries & Supercaps* **2022**, *5*, e202200043.
[45] X. Yan, Y. Yang, E. Liu, L. Sun, H. Wang, X. Z. Liao, Y. He, Z. F. Ma, *Electrochim. Acta* **2017**, *225*, 235–242.
[46] Z. Li, M. Dadsetan, J. Gao, S. Zhang, L. Cai, A. Naseri, M. E. Jimenez-Castaneda, T. Filley, J. T. Miller, M. J. Thomson, V. G. Pol, *Adv. Energy Mater.* **2021**, *11*, 2101764.
[47] R. Mogensen, S. Colbin, R. Younesi, *Batteries & Supercaps* **2021**, *4*, 791–814.
[48] Y. Ma, Y. Ma, S. L. Dreyer, Q. Wang, K. Wang, D. Goonetilleke, A. Omar, D. Mikhailova, H. Hahn, B. Breitung, T. Brezesinski, *Adv. Mater.* **2021**, *33*, 2101342.
[49] Y. He, S. L. Dreyer, Y.-Y. Ting, Y. Ma, Y. Hu, D. Goonetilleke, Y. Tang, T. Diemant, B. Zhou, P. M. Kowalski, M. Fichtner, H. Hahn, J. Aghassi-Hagmann, T. Brezesinski, B. Breitung, Y. Ma, *Angew. Chem. Int. Ed.* **2023**, e202315371 (DOI: 10.1002/anie.202315371).
[50] Y. He, S. L. Dreyer, T. Akcay, T. Diemant, R. Mönig, Y. Ma, Y. Tang, H. Wang, H. Liu, J. Lin, S. Schweidler, M. Fichtner, H. Hahn, J. Aghassi-Hagmann, T. Brezesinski, B. Breitung, Y. Ma, *manuscript in preparation*, **2024**.
[51] J. Hu, H. Tao, M. Chen, Z. Zhang, S. Cao, Y. Shen, K. Jiang, M. Zhou, *ACS Appl. Mater. Interfaces* **2022**, *14*, 12234–12242.
[52] Y. Xi, Y. Lu, *J. Power Sources* **2021**, *513*, 230554.
[53] M. Ye, S. You, J. Xiong, Y. Yang, Y. Zhang, C. C. Li, *Mater. Today Energy* **2022**, *23*, 100898.
[54] Y. Liu, Y. Qiao, W. Zhang, Z. Li, X. Ji, L. Miao, L. Yuan, X. Hu, Y. Huang, *Nano Energy* **2015**, *12*, 386–393.
[55] Y. Lu, L. Wang, J. Cheng, J. B. Goodenough, *Chem. Commun.* **2012**, *48*, 6544–6546.
[56] J. Sottmann, F. L. M. Bernal, K. V. Yusenko, M. Herrmann, H. Emerich, D. S. Wragg, S. Margadonna, *Electrochim. Acta* **2016**, *200*, 305–313.
[57] T. L. Kulova, A. M. Skundin, *Energies* **2022**, *15*, 8615.
[58] G. G. Eshetu, G. A. Elia, M. Armand, M. Forsyth, S. Komaba, T. Rojo, S. Passerini, *Adv. Energy Mater.* **2020**, *10*, 2000093.
[59] Y. Lee, J. Lee, H. Kim, K. Kang, N. S. Choi, *J. Power Sources* **2016**, *320*, 49–58.
[60] M. Piernas-Muñoz, E. Castillo-Martínez, J. L. Gómez-Cámer, T. Rojo, *Electrochim. Acta* **2016**, *200*, 123–130.
[61] G. G. Eshetu, M. Martinez-Ibañez, E. Sánchez-Diez, I. Gracia, C. Li, L. M. Rodriguez-Martinez, T. Rojo, H. Zhang, M. Armand, *Chem. Asian J.* **2018**, *13*, 2770–2780.
[62] A. Ponrouch, E. Marchante, M. Courty, J. M. Tarascon, M. R. Palacín, *Energy Environ. Sci.* **2012**, *5*, 8572–8583.
[63] A. Hofmann, Z. Wang, S. P. Bautista, M. Weil, F. Müller, R. Löwe, L. Schneider, I. U. Mohsin, T. Hanemann, *Electrochim. Acta* **2022**, *403*, 139670.
[64] K. Westman, R. Dugas, P. Jankowski, W. Wieczorek, G. Gachot, M. Morcrette, E. Irisarri, A. Ponrouch, M. R. Palacín, J. M. Tarascon, P. Johansson, *ACS Appl. Energ. Mater.* **2018**, *1*, 2671–2680.
[65] M. Goktas, C. Bolli, J. Buchheim, E. J. Berg, P. Novák, F. Bonilla, T. Rojo, S. Komaba, K. Kubota, P. Adelhelm, *ACS Appl. Mater. Interfaces* **2019**, *11*, 32844–32855.
[66] M. Á. Muñoz-Márquez, M. Zarrabeitia, S. Passerini, T. Rojo, *Adv. Mater. Interfaces* **2022**, *9*, 2101773.
[67] S. L. Dreyer, A. Kondrakov, J. Janek, T. Brezesinski, *J. Mater. Res.* **2022**, *37*, 3146–3168.
[68] P. Liu, L. Yang, B. Xiao, H. Wang, L. Li, S. Ye, Y. Li, X. Ren, X. Ouyang, J. Hu, F. Pan, Q. Zhang, J. Liu, *Adv. Funct. Mater.* **2022**, *32*, 2208586.
[69] S. Kim, H.-S. Kim, B. Kim, Y.-J. Kim, J.-W. Jung, W.-H. Ryu, *Adv. Energy Mater.* **2023**, *13*, 2301983.
[70] B. Salomez, S. Grugeon, M. Armand, P. Tran-Van, S. Laruelle, *J. Electrochem. Soc.* **2023**, *170*, 050537.

[71] L. Zhang, C. Tsolakidou, S. Mariyappan, J. M. Tarascon, S. Trabesinger, *Energy Storage Mater.* **2021**, *42*, 12–21.
[72] J. Geisler, *Online gas analysis of electrochemical reactions*, Dissertation, Humboldt-Universität Berlin, **2023**, DOI: 10.18452/26417.
[73] D. O. Ojwang, L. Häggström, T. Ericsson, J. Angström, W. R. Brant, *Dalton Trans.* **2020**, *49*, 3570–3579.
[74] M. Prieschl, J. Sedelmeier, K. Püntener, S. Hildbrand, J. D. Williams, C. O. Kappe, *J. Org. Chem.* **2023**, 9594–9598.
[75] J. M. Mcnerney, H. H. Schrenk, *Am. Ind. Hyg. Assoc. J.* **1960**, *21*, 121–124.
[76] Oxalsäuredinitril [MAK Value Documentation in German Language, 2003], 2012, Wiley-VCH, DOI: 10.1002/3527600418.mb46019d0036.
[77] H. Kim, *ACS Mater. Au* **2023**, *3*, 571–575.
[78] S. G. Patnaik, P. Adelhelm, *Prussian Blue Electrodes for Sodium-Ion Batteries, in: Sodium-Ion Batteries: Materials, Characterization, and Technology*, Eds: M.-M. Titirici, P. Adelhelm, Y.-S. Hu, 1st edition, **2023**, Wiley-VCH: Weinheim.
[79] R. Bernhard, M. Metzger, H. A. Gasteiger, *J. Electrochem. Soc.* **2015**, *162*, A1984–A1989.
[80] A. Guéguen, D. Streich, M. He, M. Mendez, F. F. Chesneau, P. Novák, E. J. Berg, *J. Electrochem. Soc.* **2016**, *163*, A1095–A1100.
[81] S. Solchenbach, M. Metzger, M. Egawa, H. Beyer, H. A. Gasteiger, *J. Electrochem. Soc.* **2018**, *165*, A3022–A3028.
[82] C. Bolli, A. Guéguen, M. A. Mendez, E. J. Berg, *Chem. Mater.* **2019**, *31*, 1258–1267.
[83] M. Metzger, B. Strehle, S. Solchenbach, H. A. Gasteiger, *J. Electrochem. Soc.* **2016**, *163*, A1219–A1225.
[84] R. Lundström, N. Gogoi, X. Hou, E. J. Berg, *J. Electrochem. Soc.* **2023**, *170*, 040516.
[85] A. T. S. Freiberg, J. Sicklinger, S. Solchenbach, H. A. Gasteiger, *Electrochim. Acta* **2020**, *346*, 136271.
[86] S. E. Renfrew, B. D. McCloskey, *J. Am. Chem. Soc.* **2017**, *139*, 17853–17860.
[87] M. Metzger, P. Walke, S. Solchenbach, G. Salitra, D. Aurbach, H. A. Gasteiger, *J. Electrochem. Soc.* **2020**, *167*, 160522.
[88] J. M. Tarascon, D. Guyomard, *Solid State Ionics* **1994**, *69*, 293–305.
[89] M. Metzger, B. Strehle, S. Solchenbach, H. A. Gasteiger, *J. Electrochem. Soc.* **2016**, *163*, A798–A809.
[90] B. B. Berkes, A. Jozwiuk, H. Sommer, T. Brezesinski, J. Janek, *Electrochem. Commun.* **2015**, *60*, 64–69.
[91] B. B. Berkes, A. Jozwiuk, M. Vračar, H. Sommer, T. Brezesinski, J. Janek, *Anal. Chem.* **2015**, *87*, 5878–5883.
[92] A. J. Demello, *ACS Sens.* **2022**, *7*, 1235–1236.
[93] M. Dong, W. Sun, C. Wu, T. Feng, L. Zhao, H. Zhang, L. Chen, X. Pei, Z. Ren, Y. Cheng, *Vacuum* **2021**, *191*, 110357.
[94] J. H. Batey, *Vacuum* **2014**, *101*, 410–415.
[95] W. R. Blanchard, P. J. McCarthy, H. F. Dylla, P. H. LaMarche, J. E. Simpkins, *J. Vac. Sci. Technol. A: Vacuum, Surfaces, and Films* **1986**, *4*, 1715–1719.
[96] A. Rudola, K. Du, P. Balaya, *J. Electrochem. Soc.* **2017**, *164*, A1098–A1109.
[97] R. L. Germscheidt, D. Da Silva Francischini, M. B. Silva, M. A. Zezzi Arruda, A. L. Barboza Formiga, T. C. Rizuti Da Rocha, J. A. Bonacin, *ACS Appl. Energ. Mater.* **2022**, *5*, 9447–9454.
[98] G. Hernández, R. Mogensen, R. Younesi, J. Mindemark, *Batteries & Supercaps* **2022**, *5*, e202100373.
[99] A. Bhide, J. Hofmann, A. Katharina Dürr, J. Janek, P. Adelhelm, *Phys. Chem. Chem. Phys.* **2014**, *16*, 1987–1998.
[100] R. Mogensen, S. Colbin, A. S. Menon, E. Björklund, R. Younesi, *ACS Appl. Energ. Mater.* **2020**, *3*, 4974–4982.
[101] R. Mogensen, A. Buckel, S. Colbin, R. Younesi, *Chem. Mater.* **2021**, *33*, 1130–1139.
[102] J. Welch, R. Mogensen, W. van Ekeren, H. Eriksson, A. J. Naylor, R. Younesi, *J. Electrochem. Soc.* **2022**, *169*, 120523.
[103] R. Sun, Y. You, *ACS Appl. Mater. Interfaces* **2023**, *15*, 44599–44606.
[104] M. Metzger, H. A. Gasteiger, *Energy Environ. Mater.* **2022**, *5*, 688–692.
[105] L. Karger, S. Korneychuk, W. van den Bergh, S. L. Dreyer, R. Zhang, A. Kondrakov, J. Janek, T. Brezesinski, *Chem. Mater.* **2023**, DOI: 10.1021/acs.chemmater.3c02727.
[106] W. E. Wallace, NIST Mass Spectrometry Data Center, https://webbook.nist.gov/cgi/inchi?ID=C74908, retrieved 04.10.2023.
[107] W. E. Wallace, NIST Mass Spectrometry Data Center, https://webbook.nist.gov/cgi/inchi?ID=C460195, retrieved 04.10.2023.
[108] R. Lundström, E. J. Berg, *J. Power Sources* **2021**, *485*, 229347.
[109] J. Wang, S. L. Dreyer, K. Wang, Z. Ding, T. Diemant, G. Karkera, Y. Ma, A. Sarkar, B. Zhou, M. V. Gorbunov, A. Omar, D. Mikhailova, V. Presser, M. Fichtner, H. Hahn, T. Brezesinski, B. Breitung, Q. Wang, *Mater. Futures* **2022**, *1*, 035104.
[110] C. A. Rego, R. S. Tsang, P. W. May, M. N. R. Ashfold, K. N. Rosser, *J. Appl. Phys.* **1996**, *79*, 7264–7273.
[111] D. Heathcote, C. Vallance, *J. Phys. B: At. Mol. Opt. Phys.* **2018**, *51*, 195203.
[112] H. Ren, Y. Li, Q. Ni, Y. Bai, H. Zhao, C. Wu, *Adv. Mater.* **2022**, *34*, 2106171.
[113] A. R. Genreith-Schriever, H. Banerjee, A. S. Menon, E. N. Bassey, L. F. J. Piper, C. P. Grey, A. J. Morris, *Joule* **2023**, *7*, 1623–1640.
[114] M. Nsangou, M. L. Senent, M. Hochlaf, *Chem. Phys.* **2009**, *355*, 164–168.
[115] F. Sebastianelli, F. Carelli, F. A. Gianturco, *Chem. Phys.* **2012**, *398*, 199–205.
[116] P. Mukherjee, N. V. Faenza, N. Pereira, J. Ciston, L. F. J. Piper, G. G. Amatucci, F. Cosandey, *Chem. Mater.* **2018**, *30*, 8431–8445.
[117] S. Oswald, D. Pritzl, M. Wetjen, H. A. Gasteiger, *J. Electrochem. Soc.* **2021**, *168*, 120501.
[118] R. Jung, M. Metzger, F. Maglia, C. Stinner, H. A. Gasteiger, *J. Electrochem. Soc.* **2017**, *164*, A1361–A1377.
[119] M. H. Cheah, P. Chernev, *Sci. Rep.* **2021**, *11*, 23058.
[120] V. V. Pavlishchuk, A. W. Addison, *Inorg. Chim. Acta* **2000**, *298*, 97–102.
[121] X. Pan, A. Chojnacka, F. Béguin, *J. Energy Chem.* **2022**, *72*, 33–40.
[122] V. Skarda, D. Ivkovich, M. M. Labes, *J. Polym. Sci. Polym. Chem. Ed.* **1985**, *23*, 107–117.
[123] T. Guo, A. Illies, V. Cammarata, M. Arndt, W. Sonzogni, *J. Electroanal. Chem.* **2007**, *610*, 102–105.
[124] S. Roberts, L. Chen, B. Kishore, C. E. J. Dancer, M. J. H. Simmons, E. Kendrick, *J. Colloid Interface Sci.* **2022**, *627*, 427–437.
[125] Y. L. Wang, H. D. Lee, M. W. Beach, D. W. Margerum, *Inorg. Chem.* **1987**, *26*, 2444–2449.
[126] D. M. Crumpton-Bregel, K. I. Goldberg, *J. Am. Chem. Soc.* **2003**, *125*, 9442–9456.
[127] W. Lau, J. C. Huffman, J. K. Kochi, *Organometallics* **1982**, *1*, 155–169.
[128] D. Dixon, S. Mangold, M. Knapp, H. Ehrenberg, A. Bhaskar, *Adv. Energy Mater.* **2021**, *11*, 2100479.
[129] E. Lee, D. E. Brown, E. E. Alp, Y. Ren, J. Lu, J. J. Woo, C. S. Johnson, *Chem. Mater.* **2015**, *27*, 6755–6764.
[130] E. McCalla, M. T. Sougrati, G. Rousse, E. J. Berg, A. Abakumov, N. Recham, K. Ramesha, M. Sathiya, R. Dominko, G. Van Tendeloo, P. Novák, J.-M. Tarascon, *J. Am. Chem. Soc.* **2015**, *137*, 4804–4814.
[131] S. Xu, Y. Wang, L. Ben, Y. Lyu, N. Song, Z. Yang, Y. Li, L. Mu, H. T. Yang, L. Gu, Y.-S. Hu, H. Li, Z.-H. Cheng, L. Chen, X. Huang, *Adv. Energy Mater.* **2015**, *5*, 1501156.
[132] A. S. Christiansen, R. E. Johnsen, P. Norby, C. Frandsen, S. Mørup, S. H. Jensen, K. K. Hansen, P. Holtappels, *J. Electrochem. Soc.* **2015**, *162*, A531–A537.
[133] G. Eggert, J. Heitbaum, *Electrochim. Acta* **1986**, *31*, 1443–1448.
[134] E. Cattaneo, J. Ruch, *J. Power Sources* **1993**, *44*, 341–347.
[135] J.-P. Schmiegel, M. Leißing, F. Weddeling, F. Horsthemke, J. Reiter, Q. Fan, S. Nowak, M. Winter, T. Placke, *J. Electrochem. Soc.* **2020**, *167*, 060516.
[136] J. Geisler, L. Pfeiffer, G. A. Ferrero, P. Axmann, P. Adelhelm, *ChemRxiv.* (Analytical Chemistry) **2023**, DOI: 10.26434/chemrxiv-2023-md389.
[137] C. Misiewicz, R. Lundström, I. Ahmed, M. J. Lacey, W. R. Brant, E. J. Berg, *J. Power Sources* **2023**, *554*, 232318.
[138] U. Mattinen, M. Klett, G. Lindbergh, R. Wreland Lindström, *J. Power Sources* **2020**, *477*, 228968.
[139] D. B. Thornton, B. J. V. Davies, S. B. Scott, A. Aguadero, M. P. Ryan, I. E. L. Stephens, *Angew. Chem. Int. Ed.* **2023**, e202315357 (DOI: 10.1002/anie.202315357).

Manuscript received: December 14, 2023
Revised manuscript received: January 12, 2024
Accepted manuscript online: January 15, 2024
Version of record online: January 31, 2024